Measuring supermassive black hole mergers with LISA

Antoine Klein

University of Birmingham

ICTS, Bangalore, December 17-19 2019

Outline

SMBHBs with LISA

Supermassive black hole binaries are one of the main science targets for the space-based interferometer LISA.

Long-lived signals with high SNRs will allow for precise measurements of various aspects of GW signals, such as spin-induced precession, multiple ringdown modes measurements, eccentricity, etc.

The high horizon distance in a broad mass range will allow for supermassive black hole evolution model selection.

SMBHB signals

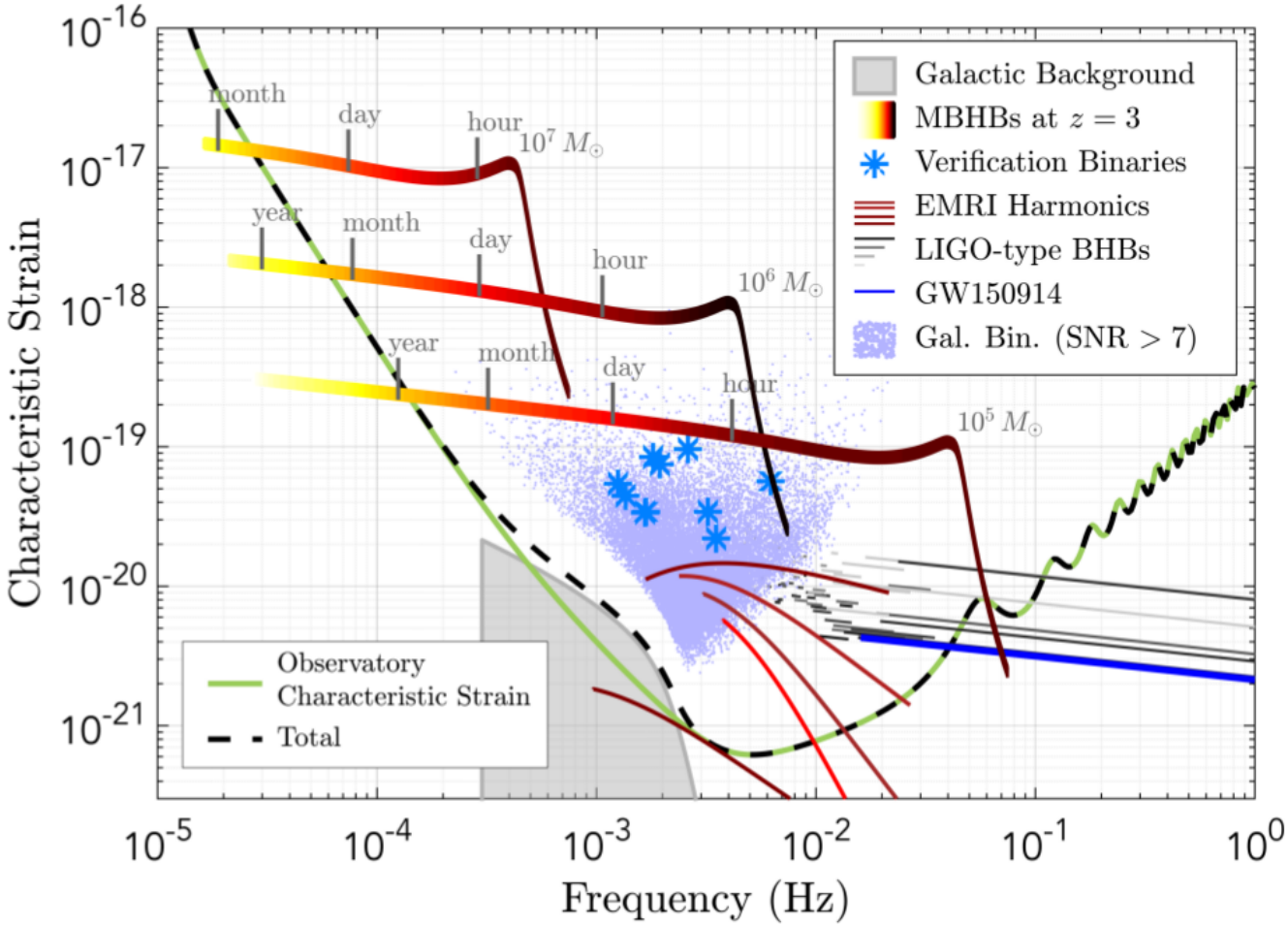

[Amaro-Seoane+ (arXiv: 1702.00786)]

Science targets

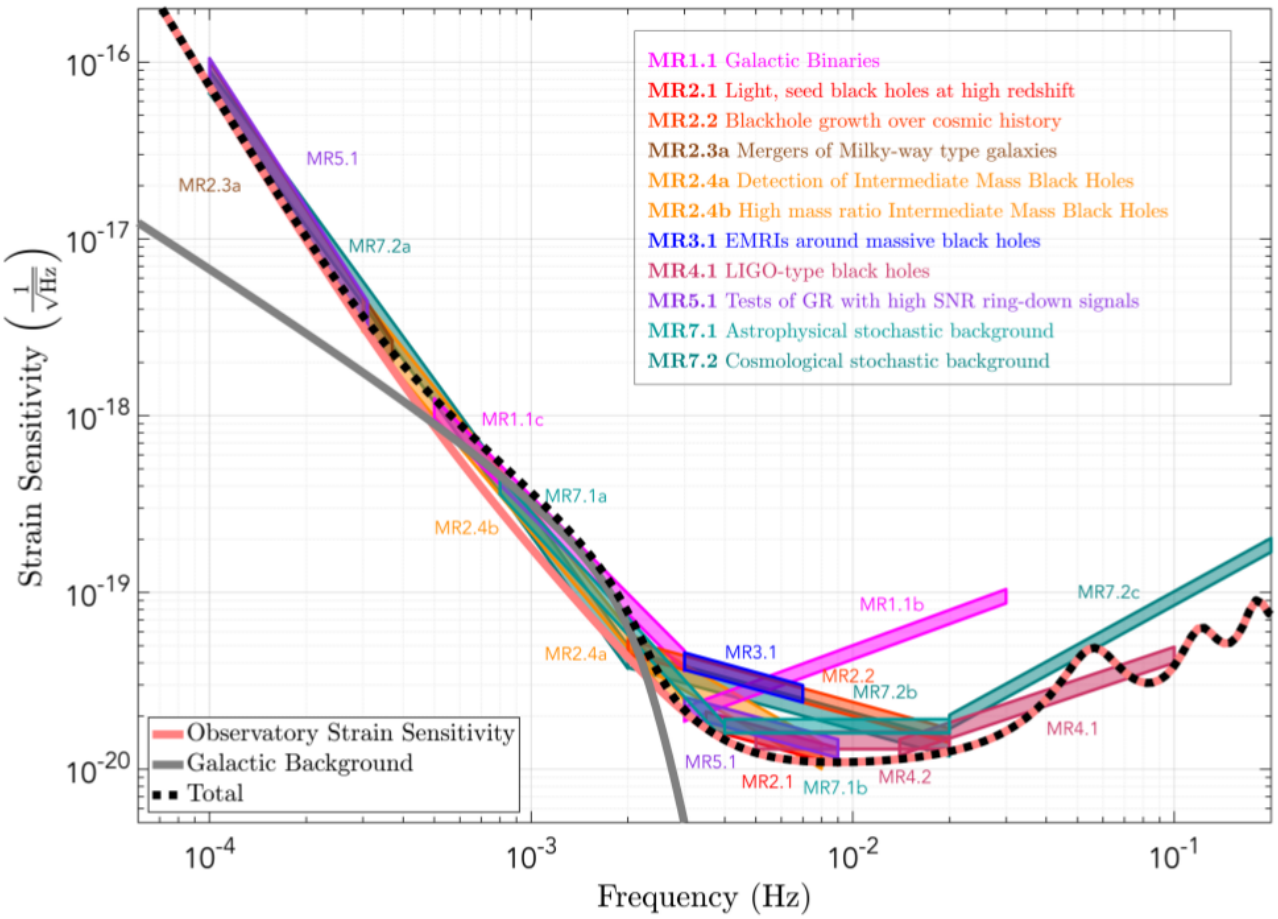

[Amaro-Seoane+ (arXiv: 1702.00786)]

Horizon distance

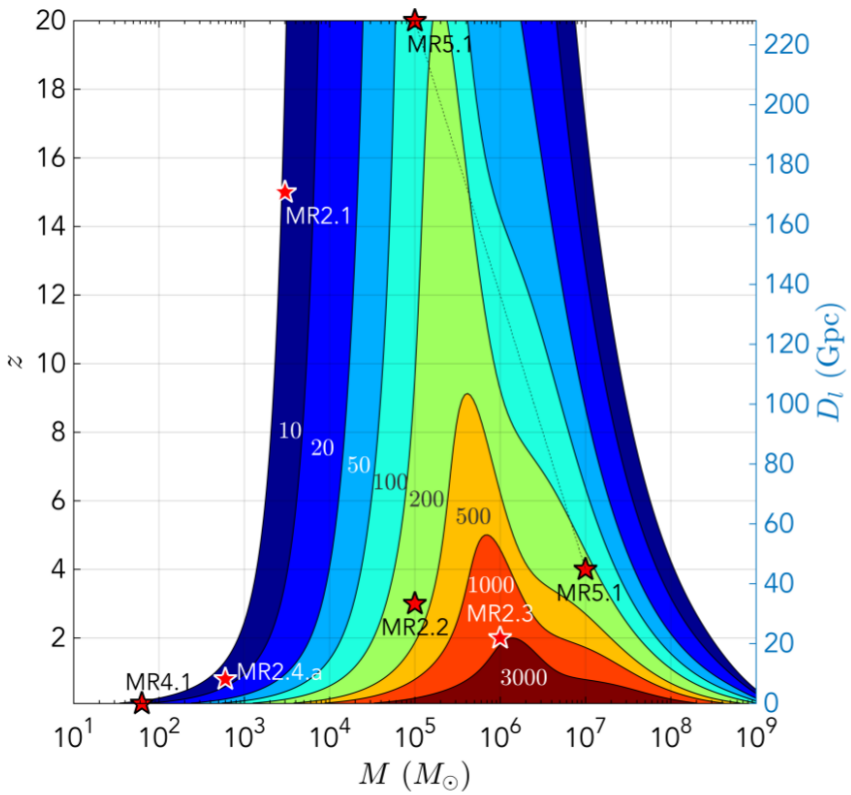

[Amaro-Seoane+ (arXiv: 1702.00786)]

Ground-Based Gravitational-Wave Detectors

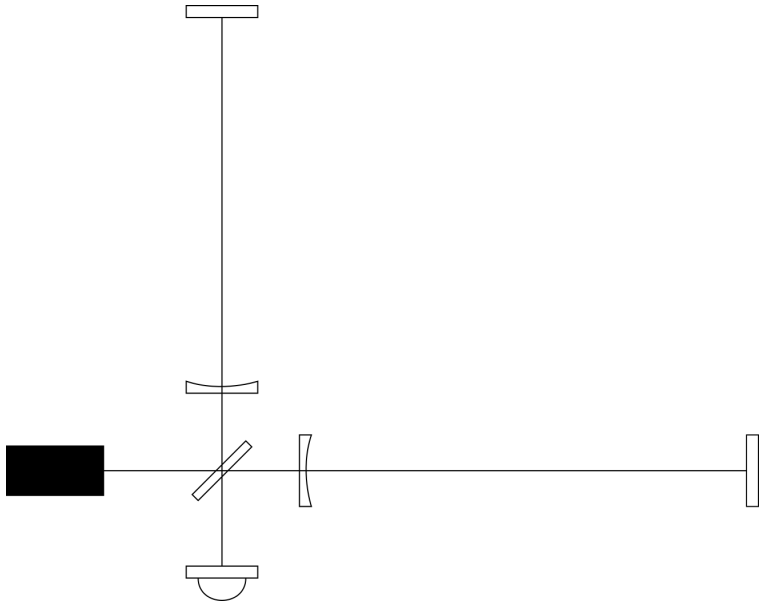

- Fixed armlengths
- Fixed geometry
- Single laser
- Static detector (-ish)

Space-Based Gravitational-Wave Detectors

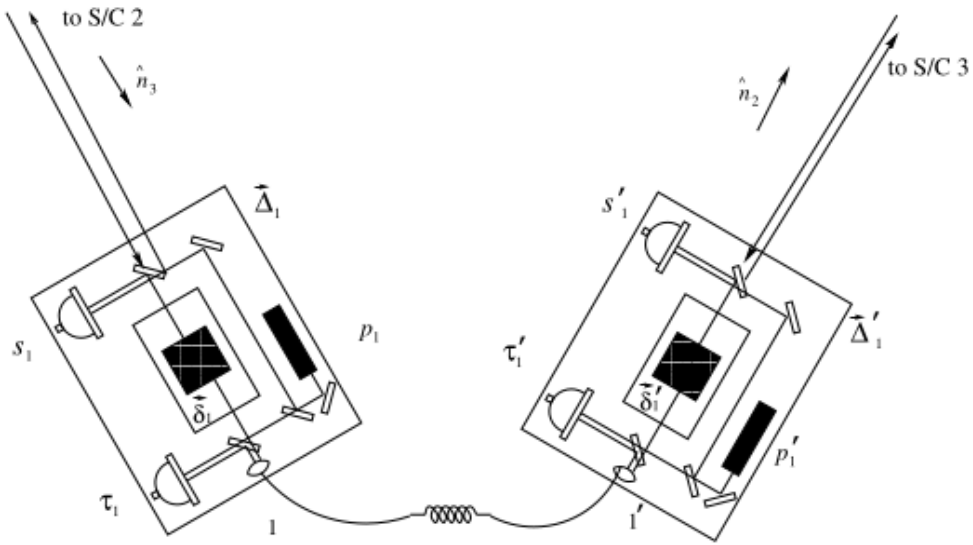

[M. Tinto, S. V. Dhurandhar, "Time-Delay Interferometry"]

- Variable armlengths
- Variable geometry
- Multiple lasers
- Moving detector

Time-Delay Interferometry

The complicated setup requires the development of a new technique to cancel out the optical noise in the data streams: time-delay interferometry.

By combining laser phase measurements from different spacecrafts at different times, we can construct combinations of those which cancel out the optical noise.

These combinations will respond to a passing gravitational wave in a specific frequency-dependent manner.

Single Arm Response

The instrument data will consist in a combination of different laser phase measurements. Therefore, we can write the instrument response to a passing gravitational wave as the acquired phase during a photon's travel from one spacecraft to the next.

$$\Delta\phi_k = \int_{\text{path}} \omega_\ell dt, \tag{1}$$

or, equivalently, the optical path length is

$$L_k = \frac{\Delta\phi_k}{\omega_\ell} = \int_{\text{path}} dt. \tag{2}$$

Single Arm Response

Assuming a gravitational wave travelling in the z direction, the spacetime through which the photon travels can be described by the metric

$$ds^2 = -dt^2 + dx^2 + dy^2 + dz^2 + h_{ab}(t,z)dx^a dx^b, \tag{3}$$

$$= -dudv + dx^2 + dy^2 + h_{ab}(u)dx^a dx^b, \tag{4}$$

with retarded time $u = t - z$, and advanced time $v = t + z$.
The photon travelling along a null geodesic, we have

$$dt^2 = dx^2 + dy^2 + dz^2 + h_{ab}dx^a dx^b. \tag{5}$$

Single Arm Response

Assuming that the photon is emitted from one spacecraft with coordinates $x^\alpha(0)$ and received at another with coordinates $x^\alpha(1)$, we can parametrize the photon path with affine parameter λ as

$$x^\alpha(\lambda) = x^\alpha(0) + \lambda r^\alpha, \tag{6}$$

$$r^\alpha = x^\alpha(1) - x^\alpha(0). \tag{7}$$

We then get along the photon path

$$dt = d\lambda \sqrt{\dot{x}^2 + \dot{y}^2 + \dot{z}^2 + h_{ab}(\lambda)\dot{x}^a\dot{x}^b} \tag{8}$$

$$= d\lambda L_0 \sqrt{1 + h_{ab}(\lambda)\hat{r}^a\hat{r}^b}. \tag{9}$$

Single Arm Response

The optical path length is

$$L_k = \int_{\text{path}} dt \tag{10}$$

$$= L_0 \int_0^1 d\lambda \left[1 + \frac{1}{2} h_{ab}(\lambda) \hat{r}^a \hat{r}^b\right]. \tag{11}$$

Single Arm Response

Using the retarded time $u = t - z$, we get

$$L_k = L_0 + \frac{L_0}{2} \int_0^1 d\lambda \, h_{ab}(\lambda) \hat{r}^a \hat{r}^b \tag{12}$$

$$= L_0 + \frac{1}{2} \frac{\hat{r}^a \hat{r}^b}{1 - \hat{\boldsymbol{z}} \cdot \hat{\boldsymbol{r}}} \int_{u_r - \Delta u}^{u_r} du \, h_{ab}(u), \tag{13}$$

when the gravitational wave travels along the $\hat{\boldsymbol{z}}$ direction.

Single Arm Response

If we define the Fourier transform of our signal

$$\tilde{h}_{ab}(f) = \int du\, h_{ab}(u) e^{2\pi i f u}, \tag{14}$$

we can rewrite the response as

$$\frac{\Delta L_{ij}}{L_0} = \int df\, \frac{1}{2} \hat{r}^a \hat{r}^b \tilde{h}_{ab}(f) \mathcal{T}(f, \hat{\boldsymbol{z}}) e^{-2\pi i f u_r}, \tag{15}$$

with transfer function

$$\mathcal{T}(f, \hat{\boldsymbol{z}}) = \mathrm{sinc}\left[\pi f L_0 \left(1 - \hat{\boldsymbol{z}} \cdot \hat{\boldsymbol{r}}\right)\right] e^{i\pi f L_0 (1 - \hat{\boldsymbol{z}} \cdot \hat{\boldsymbol{r}})}. \tag{16}$$

Single Arm Response

In particular, if we assume that the gravitational wave is monochromatic,

$$h_{ab}(u) = A_+ e^+_{ab} \cos(2\pi f_0 u) + A_\times e^\times_{ab} \sin(2\pi f_0 u), \tag{17}$$

the response becomes

$$\frac{\Delta L_{ij}(u_r)}{L_0} = \frac{1}{2}\Re\left[\mathcal{T}(f_0, \hat{\boldsymbol{z}}, u_r)\hat{r}^a(u_r)\hat{r}^b(u_r)(A_+ e^+_{ab} - iA_\times e^\times_{ab})e^{-2i\pi f_0 u_r}\right]. \tag{18}$$

LISA orbits

The spacecraft are placed in inclined eccentric orbits such that they form a configuration that stays as close to an equilateral triangle as possible as they orbit the Sun.

This is made possible by choosing

$$\iota = \sqrt{3}e, \tag{19}$$

$$e = \frac{L_0}{2\sqrt{3}R}, \tag{20}$$

and placing the perihelia equally spaced around the barycenter's orbit.

LISA orbits

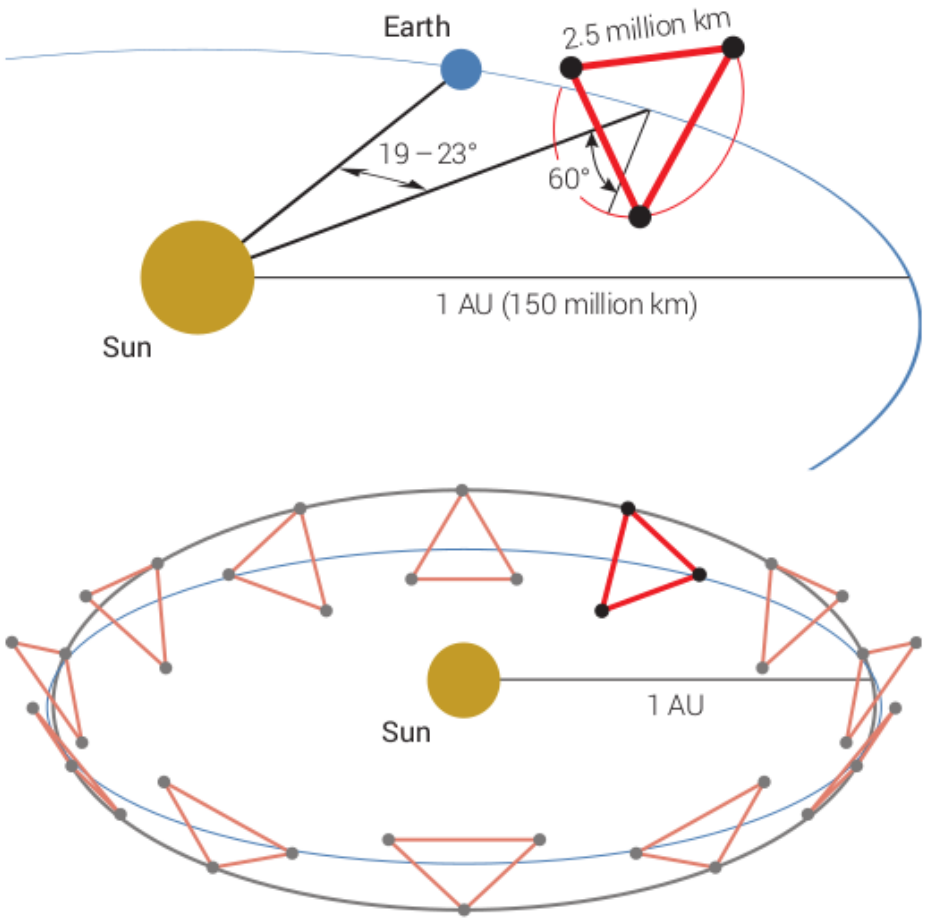

[Amaro-Seoane+ (arXiv: 1702.00786)]

Triangle Configuration

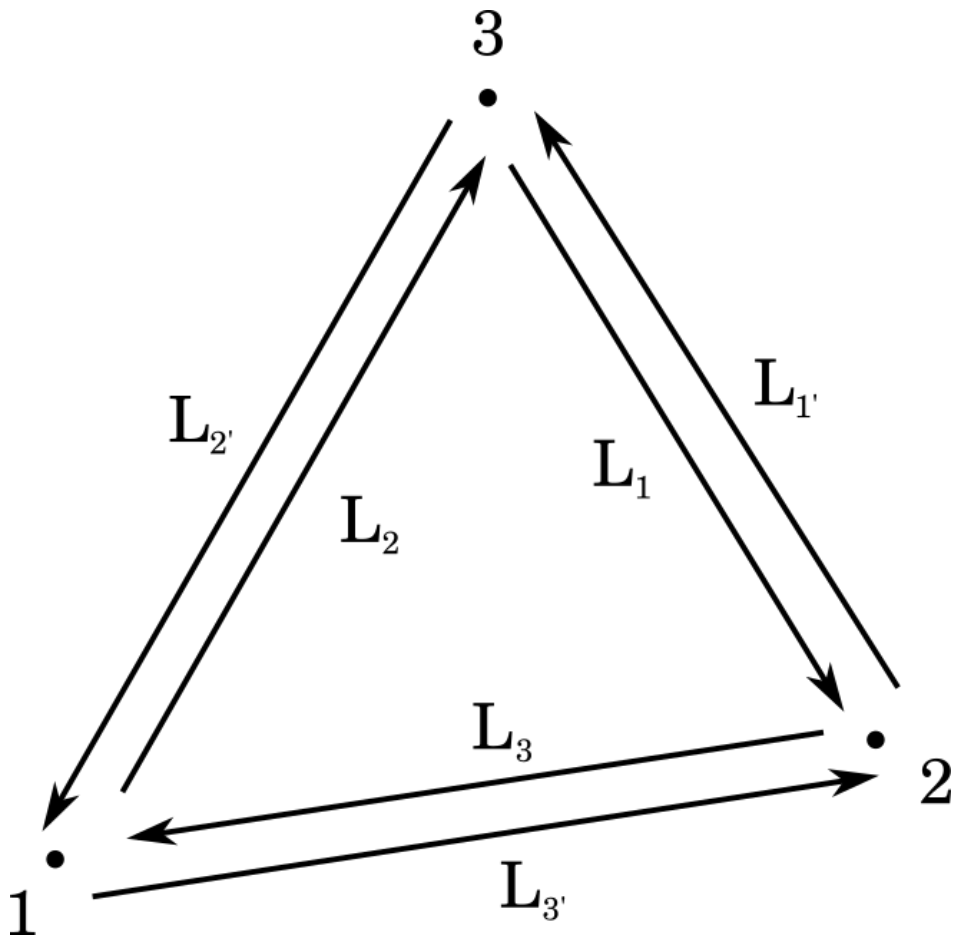

Armlengths

We can express the armlenths as a function of time by expanding the Keplerian orbits in powers of $e \sim 0.005$ and the velocities $\omega R \sim 10^{-4}$.

$$L_j(t) = L_0 + \sum_{m,n} e^m (\omega R)^n L_j^{(m,n)}(t). \tag{21}$$

At leading order, the armlengths are constant and equal.

The leading order correction corresponds to constant, unequal armlengths.

Taking into account the spacecraft velocities will lead to variable, unequal armlengths.

Single Arm TDI Variables

The LISA data will consist in six single-arm variables containing the GW signal. We can express them as $y_{ijk}(t)$, where i corresponds to the spacecraft where the signal originates, k to the spacecraft where it is measured, and j to the arm along which the signal propagates.

The optical noise contained in the y_{ijk}'s depend on three noise functions ϕ_i, as

$$N^{\mathrm{I}}[y_{ijk}(t)] = \phi_i[t - L_j(t)] - \phi_k(t). \tag{22}$$

Single Round-trip TDI Variables

Assuming that the armlengths are constant and equal, we can define a time-delay operator as

$$Dx = x(t - L). \tag{23}$$

One can build a linear combination of time delayed single-arm measurement, in such a way that it corresponds to the difference between a round trip along two arms.

$$M_X = \frac{1}{2}\left(y_{231} + Dy_{13'2} - y_{32'1} - Dy_{123}\right). \tag{24}$$

We can check that the noise in M_X cancels with the equilateral triangle assumption.

We can then build two similar TDI combinations M_Y and M_Z by permutation of the indices.

First Generation TDI Variables

Relaxing the assumption that the armlengths are equal, we can define a time-delay operator as

$$D_i x \equiv x_{,i} = x(t - L_i). \tag{25}$$

First generation TDI variables are constructed by assuming that the constellation is static on timescales comparable to a light travel around it. This results in the approximations that the armlengths are equal in both directions ($L'_i = L_i$), and that time-delay operators commute ($x_{,ij} = x_{,ji}$).

First Generation TDI Variables

One can build a TDI combination so that the noise cancels, in such a way that it corresponds to the difference between two Michelson-like interferometers.

$$\begin{aligned} X = & \, y_{231} + y_{13'2,3} + y_{32'1,3'3} + y_{123,2'3'3} \\ & - y_{32'1} - y_{123,2'} - y_{231,22'} - y_{13'2,322'} \, . \end{aligned} \tag{26}$$

We can check again that the noise in X cancels with the first generation TDI assumptions.

We can then build two similar TDI combinations Y and Z by permutation of the indices.

Second Generation TDI Variables

The first generation TDI variables are very useful to simulate data from a detector. However, in the real instrument those will not cancel the optical noise enough. In order to improve upon them, we need to relax our static constellation assumption.

We define a non-commutative time-delay operator as

$$\mathcal{D}_i x \equiv x_{;i} = x[t - L_i(t)], \tag{27}$$

$$\mathcal{D}_j(\mathcal{D}_i x) = x_{;ij} = x\{t - L_j(t) - L_i[t - L_j(t)]\}. \tag{28}$$

Second Generation TDI Variables

Relaxing our static detector assumption, one can no longer build a TDI combination so that the noise exactly cancels. However, by constructing a combination as

$$\begin{aligned} X_1 &= y_{231} + y_{13'2;3} + y_{32'1;3'3} + y_{123;2'3'3} \\ &+ y_{32'1;22'3'3} + y_{123;2'22'3'3} + y_{231;22'22'3'3} + y_{13'2;322'22'3'3} \\ &- y_{32'1} - y_{123;2'} - y_{231;22'} - y_{13'2;322'} \\ &- y_{231;3'322'} - y_{13'2;33'322'} - y_{32'1;3'33'322'} - y_{123;2'3'33'322'}. \end{aligned} \tag{29}$$

One can check that the noise in X_1 again reduces to a commutator

$$N[X_1] = [\mathcal{D}_3\mathcal{D}_{3'}\mathcal{D}_{2'}\mathcal{D}_2, \mathcal{D}_{2'}\mathcal{D}_2\mathcal{D}_3\mathcal{D}_{3'}]\phi_1. \tag{30}$$

We can build two similar TDI combinations X_2 and X_3 by permutation of the indices.

Long wavelength approximation

SMBHB signals will occur at the lower end of the frequency band. Therefore, it is sensible to derive the GW response in the low frequency limit.

Assuming that the metric perturbation is constant along the path of the light beam, we can write

$$h(y_{231}) = \frac{\Delta L_3}{L_0} \tag{31}$$

$$= \frac{1}{2L_0} \frac{\hat{L}_3^a \hat{L}_3^b}{1 - \hat{\boldsymbol{k}} \cdot \hat{\boldsymbol{L}}_3} \int_{u-\Delta u}^{u} h_{ab}(u') du' \tag{32}$$

$$= \frac{1}{2} h_{ab}(u) \hat{L}_3^a \hat{L}_3^b. \tag{33}$$

Long wavelength approximation

Therefore, the GW response in the single round-trip variable M_X can be computed with

$$M_X = \frac{1}{2}\left(y_{231} + D y_{13'2} - y_{32'1} - D y_{123}\right), \tag{34}$$

$$h(M_X) = \frac{1}{2} h_{ab}(t)\left(\hat{L}_3^a \hat{L}_3^b - \hat{L}_2^a \hat{L}_2^b\right). \tag{35}$$

Long wavelength approximation

We can compute the response in M_X, M_Y, and M_Z by expressing the geometrical factors of the metric perturbation in a frame tied to the detector.

Assuming that the detector lies in the $\hat{\boldsymbol{x}}$-$\hat{\boldsymbol{y}}$ plane, we can construct the triad $(\hat{\boldsymbol{k}}, \hat{\boldsymbol{p}}, \hat{\boldsymbol{q}})$

$$\hat{\boldsymbol{k}} = -(\sin\theta\cos\phi, \sin\theta\sin\phi, \cos\theta), \tag{36}$$

$$\hat{\boldsymbol{p}} = (\cos\theta\cos\phi, \cos\theta\sin\phi, -\sin\theta), \tag{37}$$

$$\hat{\boldsymbol{q}} = (\sin\phi, -\cos\phi, 0). \tag{38}$$

Long wavelength approximation

The metric perturbation becomes

$$h_{ab}(t) = h_+(t)e^+_{ab} + h_\times(t)e^\times_{ab}, \tag{39}$$
$$e^+_{ab} = \epsilon^+_{ab}\cos 2\psi - \epsilon^\times_{ab}\sin 2\psi, \tag{40}$$
$$e^\times_{ab} = \epsilon^+_{ab}\sin 2\psi + \epsilon^\times_{ab}\cos 2\psi, \tag{41}$$
$$\epsilon^+_{ab} = \hat{p}^a\hat{p}^b - \hat{q}^a\hat{q}^b, \tag{42}$$
$$\epsilon^\times_{ab} = \hat{p}^a\hat{q}^b + \hat{q}^a\hat{p}^b. \tag{43}$$

Long wavelength approximation

Assuming that the bisector of the $\hat{\boldsymbol{x}}$-$\hat{\boldsymbol{y}}$ angle coincides with the bisector of the opening angle between arms $\boldsymbol{L}_2$ and $\boldsymbol{L}_{3'}$, we can consider the three linear combinations of M_X, M_Y, and M_Z

$$M_I = M_X, \tag{44}$$

$$M_{II} = \frac{1}{\sqrt{3}} \left(M_Z - M_Y \right), \tag{45}$$

$$M_{III} = \frac{1}{3} \left(M_X + M_Y + M_Z \right). \tag{46}$$

Long wavelength approximation

The GW responses in those data channels will be

$$h(M_{I,II}) = F^{+}_{I,II}(\theta,\phi,\psi)h_{+}(t) + F^{\times}_{I,II}(\theta,\phi,\psi)h_{\times}(t), \tag{47}$$

$$h(M_{III}) = 0, \tag{48}$$

$$F^{+}_{I}(\theta,\phi,\psi) = \frac{\sqrt{3}}{2}\left[\frac{1}{2}\left(1+\cos^2\theta\right)\cos 2\phi\cos 2\psi - \cos\theta\sin 2\phi\sin 2\psi\right], \tag{49}$$

$$F^{\times}_{I,II}(\theta,\phi,\psi) = F^{+}_{I,II}(\theta,\phi,\psi-\pi/4), \tag{50}$$

$$F^{+,\times}_{II}(\theta,\phi,\psi) = F^{+,\times}_{I}(\theta,\phi-\pi/4,\psi). \tag{51}$$

$$\tag{52}$$

Long wavelength approximation

Thus, we see that in the long wavelength approximation, LISA is equivalent to two colocated detectors, rotated by $\pi/4$ with respect to each other, with a response suppressed by a factor $\sqrt{3}/2$ due to the opening angle between the arms.

It is worth noting that this description is valid in a frame tied to the detector, which significantly changes orientation during the observation of a signal.

Instrument setup

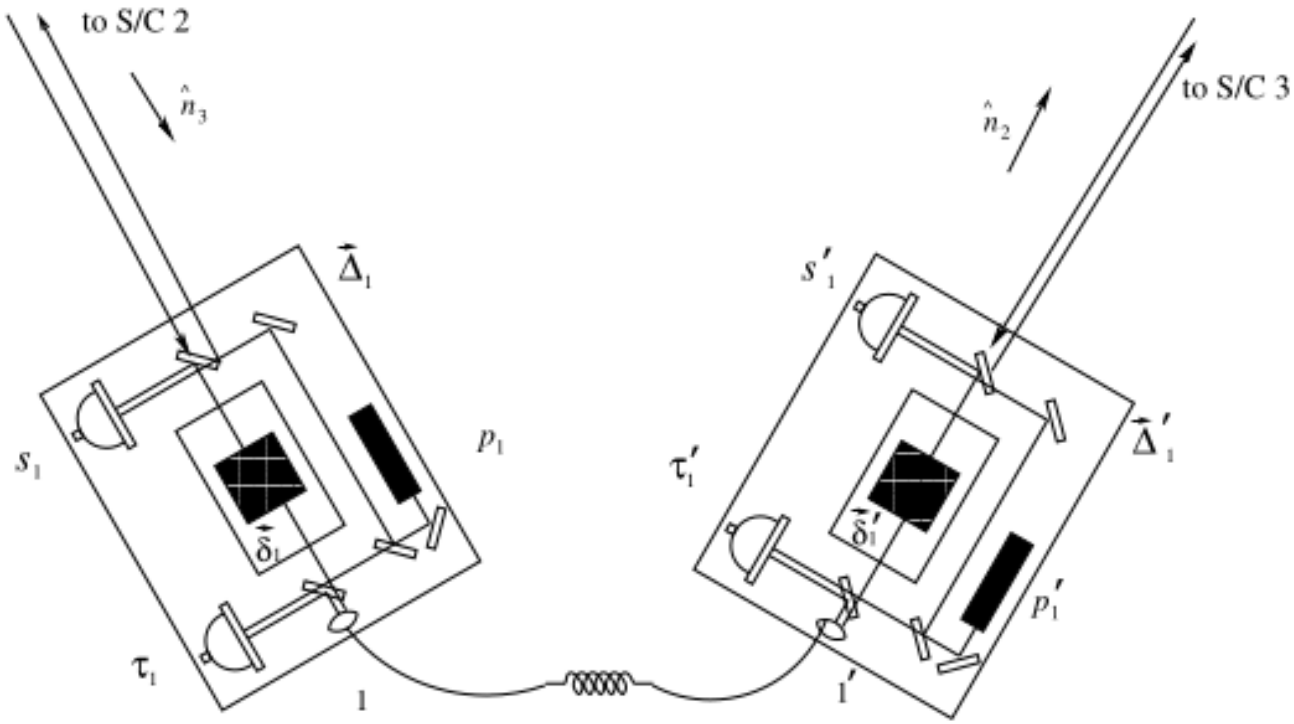

[M. Tinto, S. V. Dhurandhar, "Time-Delay Interferometry"]

Noise in single-arm variables

The noise in each single-arm variable will be dependent on three main sources:

- A component independent in each single-arm variable, dominated by laser shot noise.
- A component independent for each of the three arms, proportional to the displacement noise of the test masses.
- The laser phase noise, reduced by time-delay interferometry.

Noise in single-arm variables

We model the noise in y_{ijk} by

$$N[y_{ijk}(t)] = n^{\mathrm{s}}_j(t) + \hat{\boldsymbol{L}}_j \cdot \boldsymbol{n}^{\mathrm{a}}_j(t) - \hat{\boldsymbol{L}}_j \cdot \boldsymbol{n}^{\mathrm{a}}_{j'}(t - L_j) + n^{\mathrm{l}}_k(t) - n^{\mathrm{l}}_i(t - L_j). \tag{53}$$

We assume each noise component is Gaussian with PSD

$$\left\langle \tilde{n}^{\mathrm{l}}_j(f) \tilde{n}^{\mathrm{l}}_k(f')^* \right\rangle = S^{\mathrm{l}}_n(f) \delta_{jk} \delta(f - f'), \tag{54}$$

$$\left\langle \tilde{n}^{\mathrm{s}}_j(f) \tilde{n}^{\mathrm{s}}_k(f')^* \right\rangle = S^{\mathrm{s}}_n(f) \delta_{jk} \delta(f - f'), \tag{55}$$

$$\left\langle \tilde{n}^{\mathrm{a},m}_j(f) \tilde{n}^{\mathrm{a},n}_k(f')^* \right\rangle = S^{\mathrm{a}}_n(f) \delta_{jk} \delta_{mn} \delta(f - f'). \tag{56}$$

Noise in the single round-trip variables

The single round-trip TDI variables can be written as

$$M_X = \frac{1}{2}\left(y_{231} + Dy_{13'2} - y_{32'1} - Dy_{123}\right), \tag{57}$$

and its shot noise component will be

$$N^{\mathrm{s}}[M_X] = \frac{1}{2}\left(n^{\mathrm{s}}_3 + Dn^{\mathrm{s}}_{3'} - n^{\mathrm{s}}_{2'} - Dn^{\mathrm{s}}_2\right). \tag{58}$$

Noise in the single round-trip variables

We can compute the PSD of the shot noise component in M_X

$$S_n^{s,M_X}(f) = \int \left\langle N^s[\tilde{M}_X(f)] N^s[\tilde{M}_X(f')]^* \right\rangle df' \tag{59}$$

$$= \frac{1}{4} \int \left\langle \left(\tilde{n}_3^s + e^{2\pi i f L} \tilde{n}_{3'}^s - \tilde{n}_{2'}^s - e^{2\pi i f L} \tilde{n}_2^s \right) \times (c.c.) \right\rangle df', \tag{60}$$

$$= S_n^s(f). \tag{61}$$

Noise in the single round-trip variables

Similarly, we can compute the correlation between the noise in M_X and M_Y.

$$S_n^{\mathrm{s},M_X M_Y}(f) = \int \left\langle N^{\mathrm{s}}[\tilde{M}_X(f)] N^{\mathrm{s}}[\tilde{M}_Y(f')]^* \right\rangle df' \tag{62}$$

$$= \frac{1}{4} \int \Big\langle \left(\tilde{n}_3^{\mathrm{s}} + e^{2\pi i f L} \tilde{n}_{3'}^{\mathrm{s}} - \tilde{n}_{2'}^{\mathrm{s}} - e^{2\pi i f L} \tilde{n}_2^{\mathrm{s}} \right)$$

$$\times \left(\tilde{n}_1^{\mathrm{s}\,*} + e^{-2\pi i f' L} \tilde{n}_{1'}^{\mathrm{s}\,*} - \tilde{n}_{3'}^{\mathrm{s}\,*} - e^{-2\pi i f' L} \tilde{n}_3^{\mathrm{s}\,*} \right) \Big\rangle df', \tag{63}$$

$$= -\frac{1}{4} \int \left[e^{-2\pi i f' L} \left\langle \tilde{n}_3^{\mathrm{s}} \tilde{n}_3^{\mathrm{s}\,*} \right\rangle + e^{2\pi i f L} \left\langle \tilde{n}_{3'}^{\mathrm{s}}, \tilde{n}_{3'}^{\mathrm{s}\,*} \right\rangle \right] df', \tag{64}$$

$$= -\frac{1}{2} \cos(2\pi f L) S_n^{\mathrm{s}}(f). \tag{65}$$

Noise in the single round-trip variables

We can compute the acceleration noise in M_X.

$$N^{\mathrm{a}}[M_X] = \frac{1}{2}\Big[\hat{\boldsymbol{L}}_3 \cdot (\boldsymbol{n}^{\mathrm{a}}_3 - D\boldsymbol{n}^{\mathrm{a}}_{3'}) + \hat{\boldsymbol{L}}_{3'} \cdot \left(D\boldsymbol{n}^{\mathrm{a}}_{3'} - D^2\boldsymbol{n}^{\mathrm{a}}_3\right) - \hat{\boldsymbol{L}}_{2'} \cdot (\boldsymbol{n}^{\mathrm{a}}_{2'} - D\boldsymbol{n}^{\mathrm{a}}_2) - \hat{\boldsymbol{L}}_2 \cdot \left(D\boldsymbol{n}^{\mathrm{a}}_2 - D^2\boldsymbol{n}^{\mathrm{a}}_{2'}\right)\Big] \tag{66}$$

$$= \frac{1}{2}\hat{\boldsymbol{L}}_3 \cdot \left(\boldsymbol{n}^{\mathrm{a}}_3 + D^2\boldsymbol{n}^{\mathrm{a}}_3\right) + \frac{1}{2}\hat{\boldsymbol{L}}_2 \cdot \left(\boldsymbol{n}^{\mathrm{a}}_{2'} + D^2\boldsymbol{n}^{\mathrm{a}}_{2'}\right) - \hat{\boldsymbol{L}}_3 \cdot D\boldsymbol{n}^{\mathrm{a}}_{3'} - \hat{\boldsymbol{L}}_2 \cdot D\boldsymbol{n}^{\mathrm{a}}_2. \tag{67}$$

Noise in the single round-trip variables

Thus, the acceleration noise PSD in M_X will be

$$S_n^{\mathrm{a},M_X}(f) = \int \left\langle N^{\mathrm{a}}[\tilde{M}_X(f)] N^{\mathrm{a}}[\tilde{M}_X(f')]^* \right\rangle df' \tag{68}$$

$$= S_n^{\mathrm{a}}(f) \Bigg[\frac{1}{4} \left(|\hat{\boldsymbol{L}}_3|^2 + |\hat{\boldsymbol{L}}_2|^2 \right) \left(1 + e^{4\pi i f L} \right) \left(1 + e^{-4\pi i f L} \right)$$

$$+ \left(|\hat{\boldsymbol{L}}_3|^2 + |\hat{\boldsymbol{L}}_2|^2 \right) \Bigg] \tag{69}$$

$$= S_n^{\mathrm{a}}(f) \left[2\cos^2(2\pi f L) + 2 \right]. \tag{70}$$

Noise in the single round-trip variables

Finally, we can compute the acceleration noise correlation between M_X and M_Y. We have

$$N^{\mathrm{a}}[M_X] = \frac{1}{2}\hat{\boldsymbol{L}}_3 \cdot \left(\boldsymbol{n}^{\mathrm{a}}_3 + D^2\boldsymbol{n}^{\mathrm{a}}_3\right) + \frac{1}{2}\hat{\boldsymbol{L}}_2 \cdot \left(\boldsymbol{n}^{\mathrm{a}}_{2'} + D^2\boldsymbol{n}^{\mathrm{a}}_{2'}\right) - \hat{\boldsymbol{L}}_3 \cdot D\boldsymbol{n}^{\mathrm{a}}_{3'} - \hat{\boldsymbol{L}}_2 \cdot D\boldsymbol{n}^{\mathrm{a}}_2, \tag{71}$$

$$N^{\mathrm{a}}[M_Y] = \frac{1}{2}\hat{\boldsymbol{L}}_1 \cdot \left(\boldsymbol{n}^{\mathrm{a}}_1 + D^2\boldsymbol{n}^{\mathrm{a}}_1\right) + \frac{1}{2}\hat{\boldsymbol{L}}_3 \cdot \left(\boldsymbol{n}^{\mathrm{a}}_{3'} + D^2\boldsymbol{n}^{\mathrm{a}}_{3'}\right) - \hat{\boldsymbol{L}}_1 \cdot D\boldsymbol{n}^{\mathrm{a}}_{1'} - \hat{\boldsymbol{L}}_3 \cdot D\boldsymbol{n}^{\mathrm{a}}_3. \tag{72}$$

Noise in the single round-trip variables

Thus, the acceleration noise correlation between M_X and M_Y will be

$$S_n^{\mathrm{a},M_X M_Y}(f) = \int \left\langle N^{\mathrm{a}}[\tilde{M}_X(f)] N^{\mathrm{a}}[\tilde{M}_Y(f')]^* \right\rangle df' \tag{73}$$

$$= -\frac{1}{2} S_n^{\mathrm{a}}(f) \Bigg[|\hat{\boldsymbol{L}}_3|^2 \left(1 + e^{4\pi i f L}\right) e^{-2\pi i f L}$$

$$+ |\hat{\boldsymbol{L}}_3|^2 \left(1 + e^{-4\pi i f L}\right) e^{2\pi i f L} \Bigg] \tag{74}$$

$$= -2 S_n^{\mathrm{a}}(f) \cos(2\pi f L). \tag{75}$$

Uncorrelated channels

The noise in the channels that we have defined so far is correlated. One way around that is to express a linear combination of those channels and try to diagonalize the noise correlation matrix. We can write, in the Fourier domain,

$$\eta = a_1 \tilde{M}_X + a_2 \tilde{M}_Y + a_3 \tilde{M}_Z. \tag{76}$$

Uncorrelated channels

The SNR in η is

$$\rho^2_\eta = 4\int_0^\infty \frac{|\tilde{h}_\eta(f)|^2}{S_n^\eta(f)}df \tag{77}$$

$$= 4\int_0^\infty (a_1\tilde{h}_{M_X}, a_2\tilde{h}_{M_Y}, a_3\tilde{h}_{M_Z})C^{-1}(a_1\tilde{h}_{M_X}, a_2\tilde{h}_{M_Y}, a_3\tilde{h}_{M_Z})^\dagger df, \tag{78}$$

$$C = \begin{pmatrix} S_n^{M_X}(f) & S_n^{M_X M_Y}(f) & S_n^{M_X M_Z}(f) \\ S_n^{M_Y M_X}(f) & S_n^{M_Y}(f) & S_n^{M_Y M_Z}(f) \\ S_n^{M_Z M_X}(f) & S_n^{M_Z M_Y}(f) & S_n^{M_Z}(f) \end{pmatrix}. \tag{79}$$

Uncorrelated channels

Due to the symmetries in our setup, the noise PSD in each channel will be equal, the noise correlation between two channels will be equal, and real. The noise correlation matrix will thus be of the form

$$C = \begin{pmatrix} a & b & b \\ b & a & b \\ b & b & a \end{pmatrix}. \tag{80}$$

This matrix having rank 3, we find that a system of TDI variables from spacecraft in a triangle configuration exchanging laser signals is equivalent to three detectors with uncorrelated noise.

Uncorrelated channels

This matrix has one two-dimensional and one one-dimensional eigenspaces. A basis of eigenvectors can be chosen as

$$\boldsymbol{v}_A = \frac{1}{\sqrt{2}}(0,-1,1), \quad \boldsymbol{v}_E = \frac{1}{\sqrt{6}}(2,-1,-1), \quad \boldsymbol{v}_T = \frac{1}{\sqrt{3}}(1,1,1), \tag{81}$$

corresponding to the noise-uncorrelated TDI combinations

$$A_M = \frac{1}{\sqrt{2}}\left(\tilde{M}_Z - \tilde{M}_Y\right) = \sqrt{\frac{3}{2}}\tilde{M}_{II}, \tag{82}$$

$$E_M = \frac{1}{\sqrt{6}}\left(2\tilde{M}_X - \tilde{M}_Y - \tilde{M}_Z\right) = \sqrt{\frac{3}{2}}\left(\tilde{M}_I - \tilde{M}_{III}\right), \tag{83}$$

$$T_M = \frac{1}{\sqrt{3}}\left(\tilde{M}_X + \tilde{M}_Y + \tilde{M}_Z\right) = \sqrt{3}\tilde{M}_{III}. \tag{84}$$

As $\boldsymbol{v}_A$ and $\boldsymbol{v}_E$ are part of the same eigenspace, the noise PSD in A_M and E_M are equal.

Noise in the uncorrelated channels

The eigenvalues of the noise correlation matrix will give the noise PSD in the uncorrelated channels A_M, E_M, and T_M. We find

$$S_n^{A_M}(f) = S_n^{E_M}(f) = S_n^{M_X}(f) - S_n^{M_X,M_Y}(f) \tag{85}$$

$$= \frac{1}{2}\{[6 + 4\cos(2\pi fL) + 2\cos(4\pi fL)]S_n^{\mathrm{a}}(f) + [2 + \cos(2\pi fL)]S_n^{\mathrm{s}}(f)\}, \tag{86}$$

$$S_n^{T_M}(f) = S_n^{M_X}(f) + 2S_n^{M_X,M_Y}(f) = \sin^2(\pi fL)\left[4\sin^2(\pi fL)S_n^{\mathrm{a}}(f) + S_n^{\mathrm{s}}(f)\right]. \tag{87}$$

Contributions to the SNR

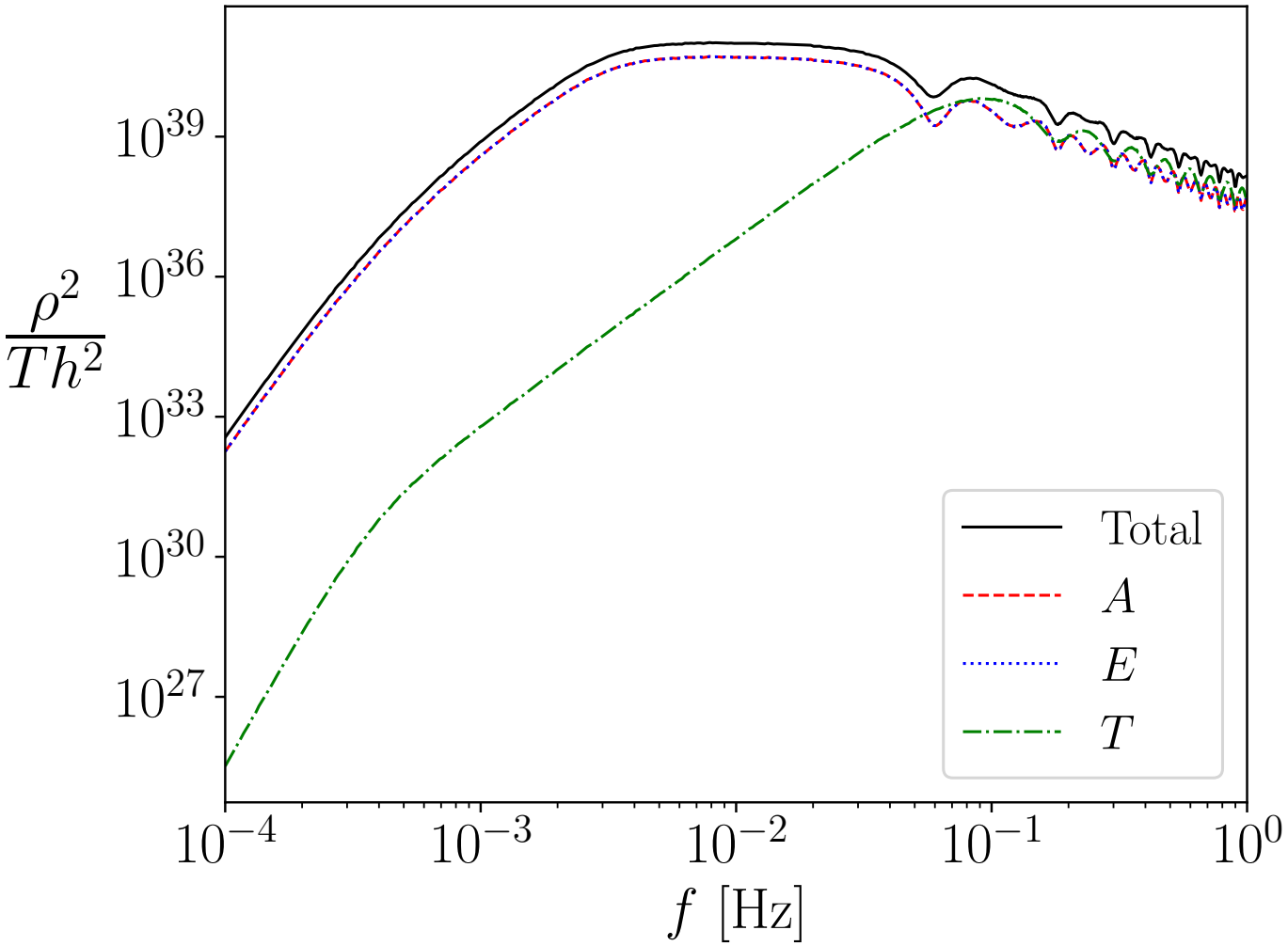

Noise in the low-frequency limit

We found two combinations of M_X, M_Y, and M_Z that have nonvanishing GW response and uncorrelated noise in the low-frequency limit, A_M and E_M.

Their response is proportional to the response in the low-frequency channels we constructed, $h(A_M) \sim h(\tilde{M}_{II})$, $h(E_M) \sim h(\tilde{M}_I)$. To compute the noise PSD to use in those channels, we can simply take the limit

$$\begin{aligned} S_n^{M_{I,II}}(f) = \frac{1}{3}\Bigg\{ & \left[\lim_{f\to 0} 6 + 4\cos(2\pi fL) + 2\cos(4\pi fL)\right] S_n^{\mathrm{a}}(f) \\ & + \left[\lim_{f\to 0} 2 + \cos(2\pi fL)\right] S_n^{\mathrm{s}}(f)\Bigg\} \\ & = 4S_n^{\mathrm{a}}(f) + S_n^{\mathrm{s}}(f). \end{aligned} \tag{88}$$

Noise in the first generation variables

To estimate the noise in the first generation variables, we can observe that the dominant contribution can be estimated with the equilateral triangle approximation. In this case, we find that

$$X = 2(1 - D^2)M_X, \tag{89}$$

$$\begin{aligned}\tilde{X} &= 2\left(1 - e^{4\pi i f L}\right)\tilde{M}_X \\ &= 4ie^{2\pi i f L}\sin(2\pi f L)\tilde{M}_X.\end{aligned} \tag{90}$$

So, we find that

$$S_n^X(f) = 16\sin^2(2\pi f L)S_n^{M_X}(f), \tag{91}$$

and similarly for the correlations. We can thus build similar uncorrelated noise channels.

Noise in the second generation variables

In the second generation variables, the same applies, and we find

$$X_1 = (1 - D^4)X, \tag{92}$$

$$\tilde{X}_1 = 2ie^{4\pi i f L} \sin(4\pi f L)\tilde{X}. \tag{93}$$

The noise PSDs and correlations will thus satisfy

$$S_n^{X_1}(f) = 4\sin^2(4\pi f L) S_n^X(f). \tag{94}$$

Residual laser phase noise

We can compute the PSD of each noise component in each TDI variable with different assumptions for the time delays:

- Assuming constant equal armlengths

$$M_X = \frac{1}{2}\left(y_{231} + Dy_{13'2} - y_{32'1} - Dy_{123}\right). \tag{95}$$

- Assuming different armlengths, ignoring spacecraft velocities

$$M_X = \frac{1}{2}\left(y_{231} + y_{13'2,3} - y_{32'1} - y_{123,2'}\right). \tag{96}$$

- Using exact armlengths

$$M_X = \frac{1}{2}\left(y_{231} + y_{13'2;3} - y_{32'1} - y_{123;2'}\right). \tag{97}$$

Residual laser phase noise

We have the freedom to make different assumptions for the time delays we use to construct the TDI variables, but the time delays present in the noise response of the single-arm variables y_{ijk} are physical, so we need to use exact time delays to estimate the residual laser phase noise in those.

In order to compute their effect in the Fourier domain, we recall

$$\begin{aligned} L_j(t) &= L_0 + \sum_{m,n} e^m (\omega R)^n L_j^{(m,n)}(t) \\ &= L_0 + \Delta L_j(t). \end{aligned} \tag{98}$$

Residual laser phase noise

Since $f\Delta L_j$ is small and periodic, we can Taylor expand the following factor, and then decompose it in a Fourier series

$$e^{2\pi i f \Delta L_j(t)} = \sum_k \frac{(2\pi i f)^k}{k!} \Delta L_j(t)^k \tag{99}$$

$$= \sum_p C_{p,j}(f) e^{2\pi i p n t}, \tag{100}$$

Residual laser phase noise

We find

$$\mathcal{F}(\mathcal{D}_j h)(f) = \int h[t - L_j(t)] e^{2\pi i f t} dt \tag{101}$$

$$= \int h(t) e^{2\pi i f [t + L_0 + \Delta L_j(t)]} dt \tag{102}$$

$$= e^{2\pi i f L_0} \int h(t) \sum_p C_{p,j}(f) e^{2\pi i p n t} e^{2\pi i f t} dt \tag{103}$$

$$= e^{2\pi i f L_0} \sum_p C_{p,j}(f) \tilde{h}(f + pn). \tag{104}$$

Residual laser phase noise in M_X

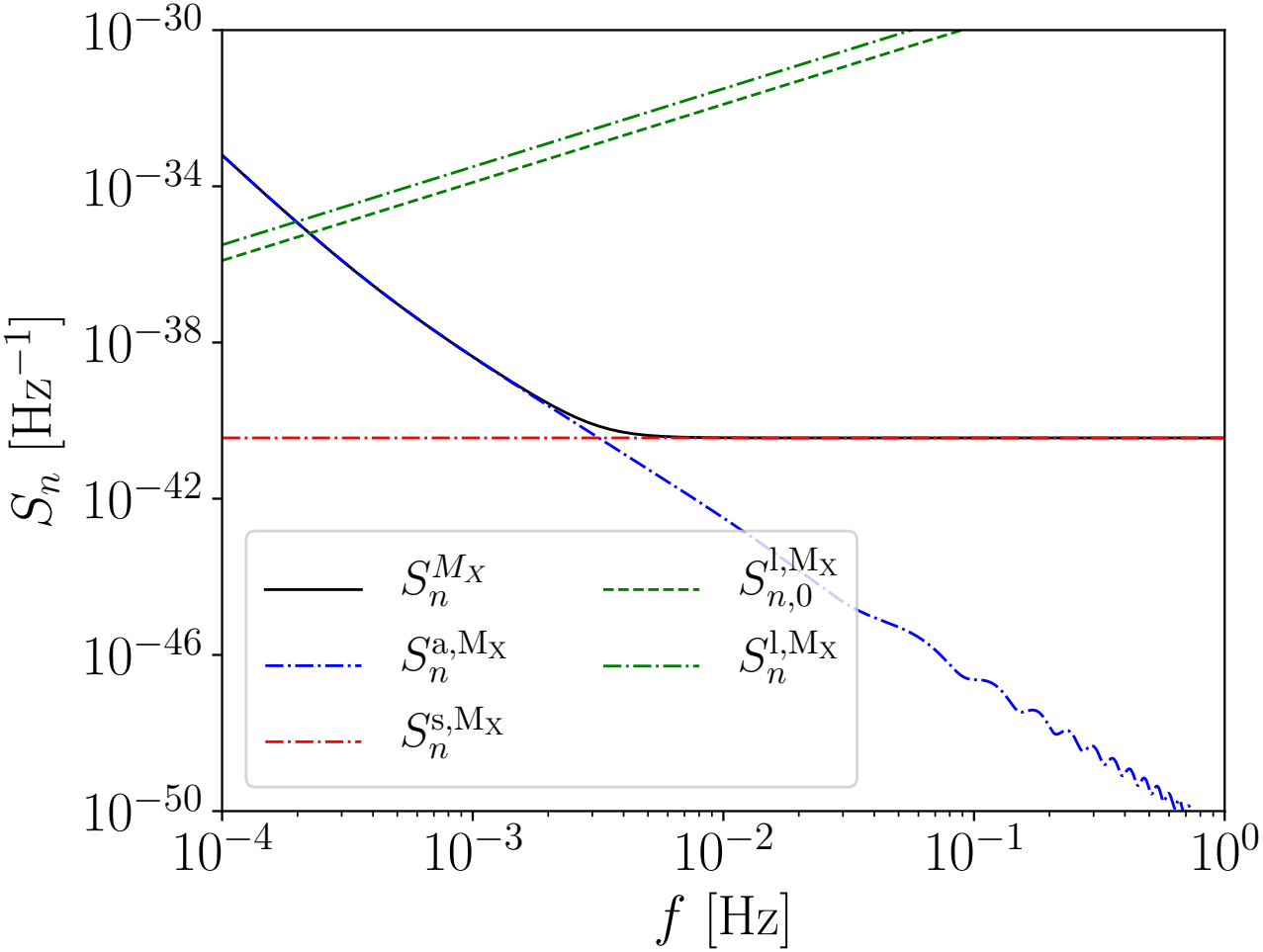

Residual laser phase noise in X

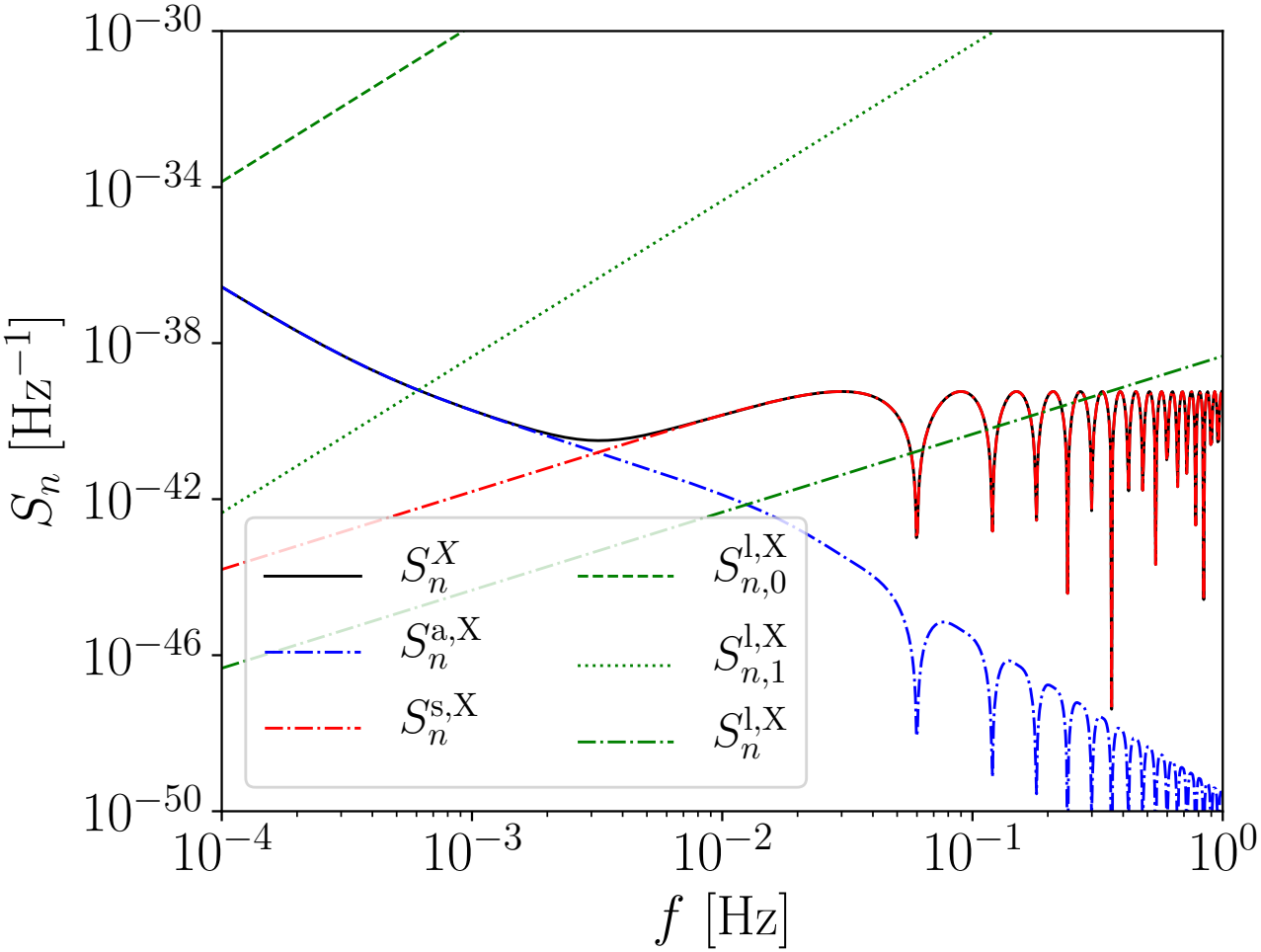

Residual laser phase noise in X_1

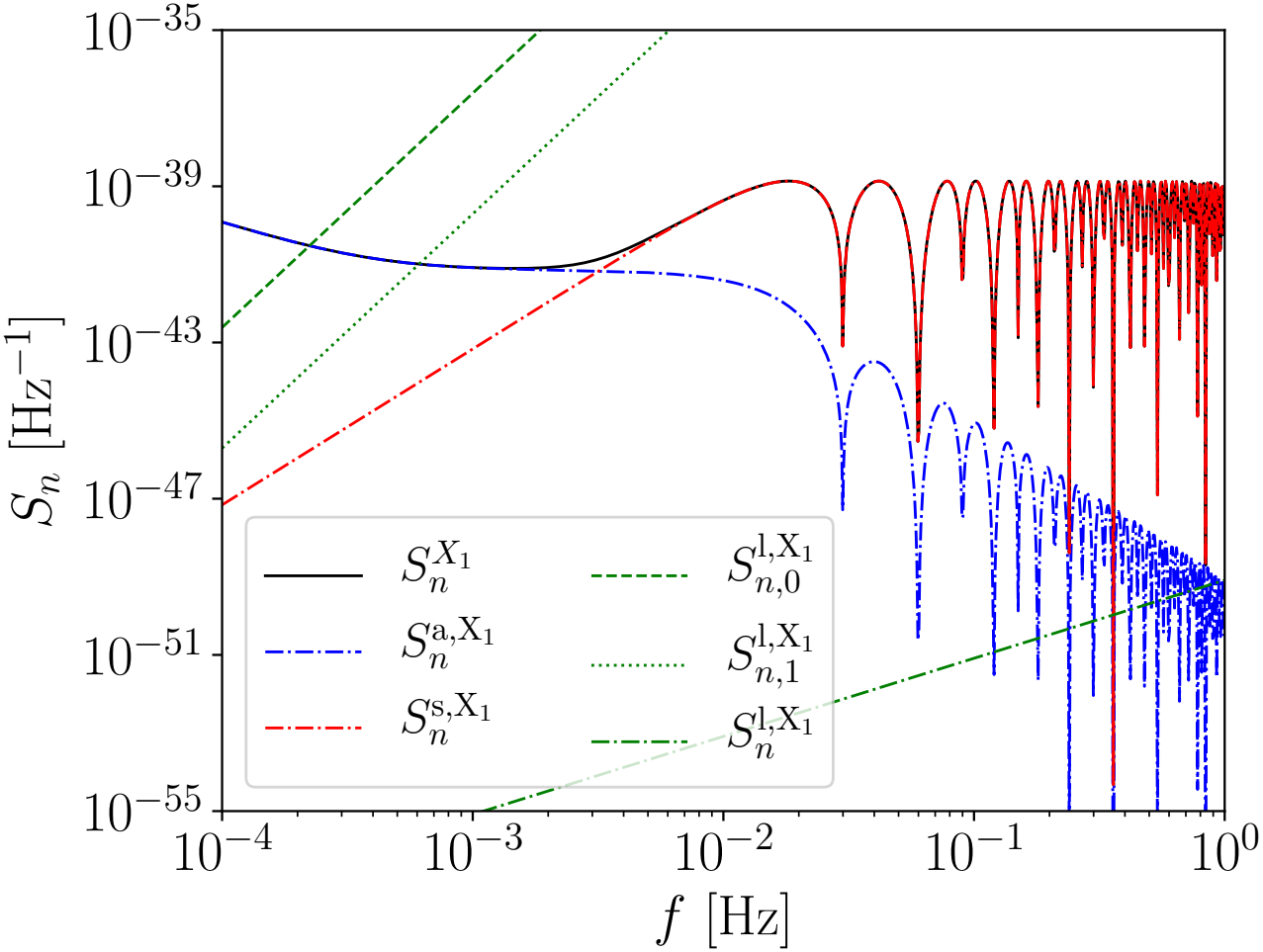

Summary of the LISA response

The modelling of the noise response shows that time-delay interferometry will be able to provide a reduction of the laser phase noise in the LISA data, provided that we use second-generation TDI variables with exact time delays.

If this is implemented, the laser phase noise becomes negligible with respect to the acceleration and shot noises.

At leading order in the spacecraft orbital eccentricity and velocities, the Fourier domain TDI variables in different generations are multiple of each other.

For this reason, performing data analysis using either generation TDI variables is equivalent, provided that the data is devoid of laser phase noise.

Inspiral waveform

The GW signal emitted by a binary system can be written as a metric perturbation depending on two polarizations

$$h_{ab}(t) = h_{+}(t)e^{+}_{ab} + h_{\times}(t)e^{\times}_{ab}. \tag{105}$$

The structure of the polarizations $h_{+}(t)$ and $h_{\times}(t)$ can be written as a series of harmonics of the orbital phase

$$h_{+,\times}(t) = \frac{GMx}{D_c c^2} \sum_n A^{(n)}_{+,\times}(t) e^{-in\phi(t)} + c.c., \tag{106}$$

$$x = \left(\frac{GM\omega}{c^3}\right)^{2/3}. \tag{107}$$

Redshift effect

The GW signal from a binary will be affected by redshift. So, the intrinsic frequency of the system will not be directly observable. Instead, the signal will imply a rescaling of the masses as

$$x = \left(\frac{GM\omega_{\rm src}}{c^3}\right)^{2/3} = \left(\frac{GM_z\omega_{\rm obs}}{c^3}\right)^{2/3}, \tag{108}$$

$$\omega_{\rm obs} = \frac{\omega_{\rm src}}{1+z}, \tag{109}$$

$$M_z = (1+z)M. \tag{110}$$

This implies that the signal can be expressed as depending on the luminosity distance instead of the comoving distance

$$h_{+,\times}(t) = \frac{GM_z x}{D_L c^2}\sum_n A^{(n)}_{+,\times}(t)e^{-in\phi(t)} + c.c., \tag{111}$$

$$D_L = (1+z)D_c. \tag{112}$$

Spin precession

Binaries with misaligned spins will experience orbital precession.
Along the evolution of the system, the orbital plane precesses, inducing a modulation of the gravitational waveform.

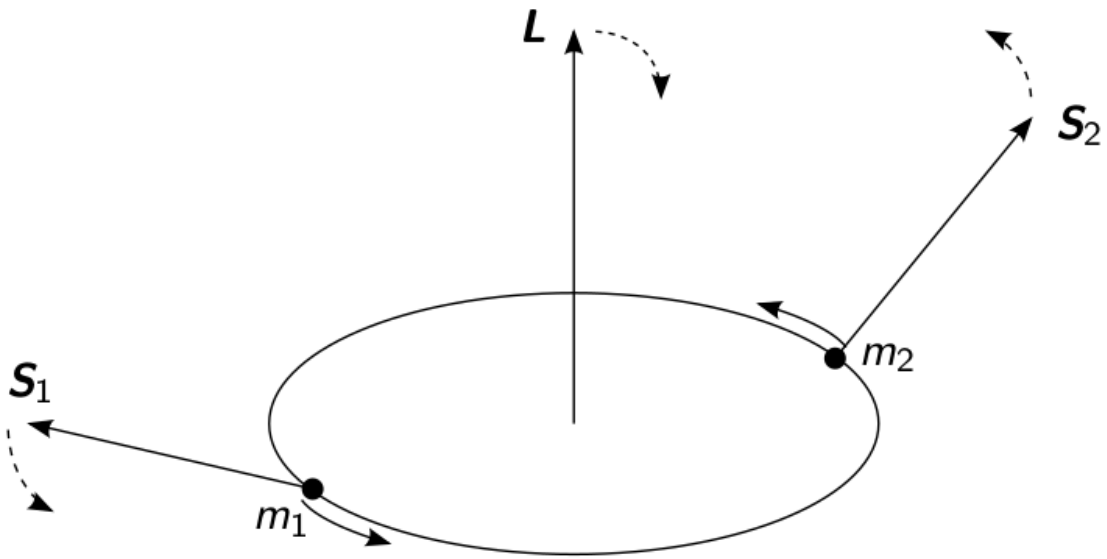

Eccentricity

Binaries on eccentric orbits will experience periastron precession, introducing an extra timescale in the problem.

The periastron-to-periastron frequency is close to the orbital frequency, generating a splitting of the harmonics in the Fourier domain.

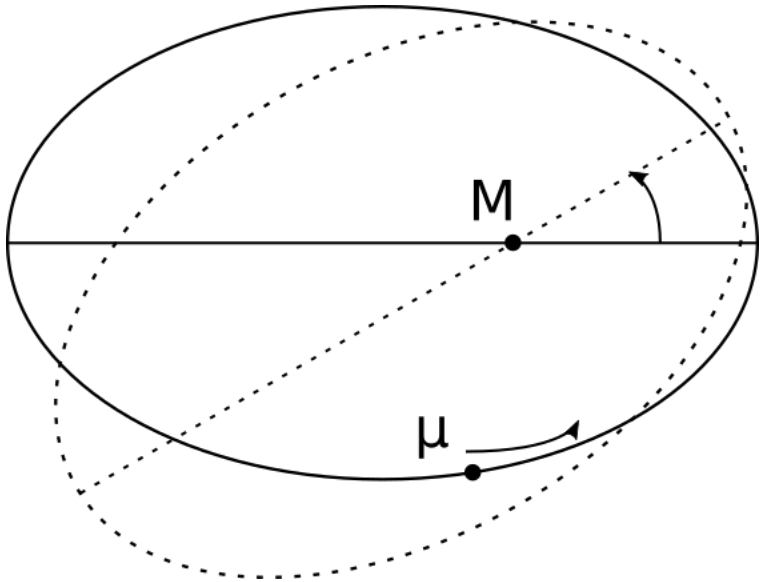

Ringdown

After the merger, a remnant black hole remains, deformed by the merger process.

It quickly radiates extra energy in gravitational waves, in order to reach a final state of a Kerr black hole.

The radiation takes the form of a series of damped modes, characterized by their frequency and damping timescale

$$h_{+,\times}(t) = \sum_{\ell,m,n} A^{\ell,m,n}_{+,\times} e^{i\omega_{\ell,m,n} t} e^{-t/\tau_{\ell,m,n}}. \tag{113}$$

The frequencies and damping timescales depend on two parameters: the mass and the spin of the remnant black hole.

Detection timescale

The accumulation of the SNR in the instrument will not be accumulated uniformly. Instead, most of the signal will be observed in the last few moments.

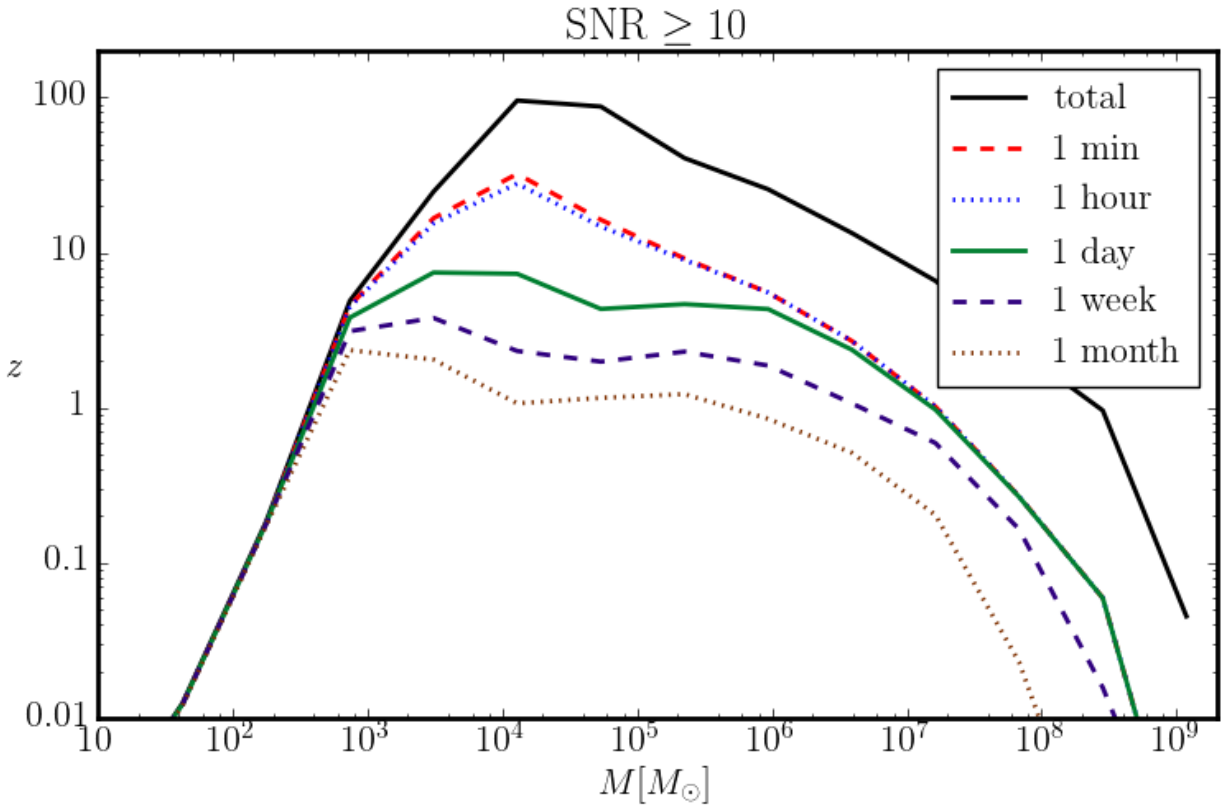

Astrophysical study

We studied two different black hole seeds scenarios:

Light seeds: popIII remnants, black holes form with initial masses around $200 M_{\odot}$ between redshifts 15 and 20.

Heavy seeds: black holes are present with masses around $10^5 M_{\odot}$ between redshifts 15 and 20.

Delay between galaxy merger and black hole merger can be important, as black holes can be driven to the center of the merged galaxy on timescales of a few Gyrs.

In the light seeds scenario, the impact of the delays does not affect the SMBHB detections significantly.

Models

We simulated the merger rate as a function of mass and redshift in three scenarios: light seeds, heavy seeds without delays, heavy seeds with delays.

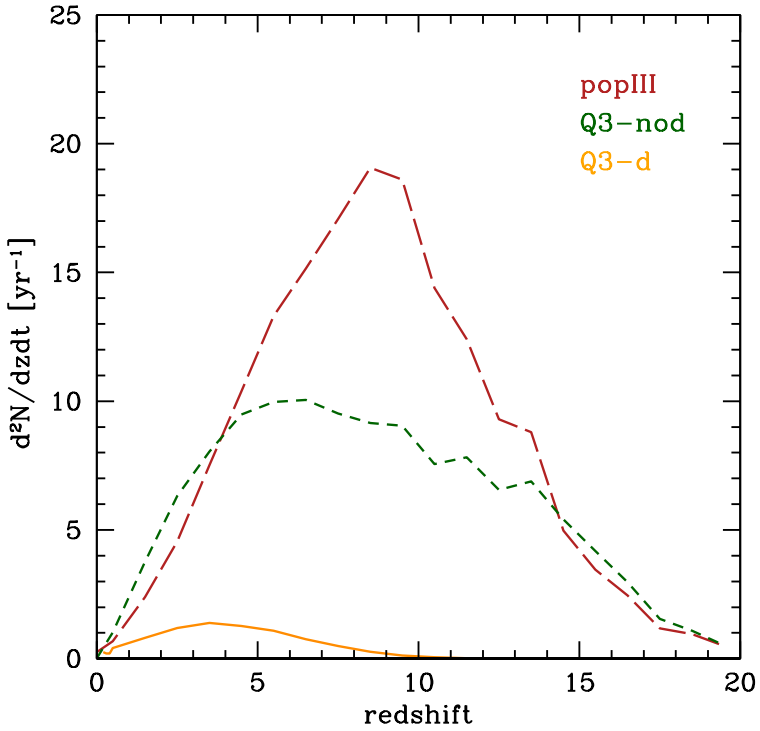

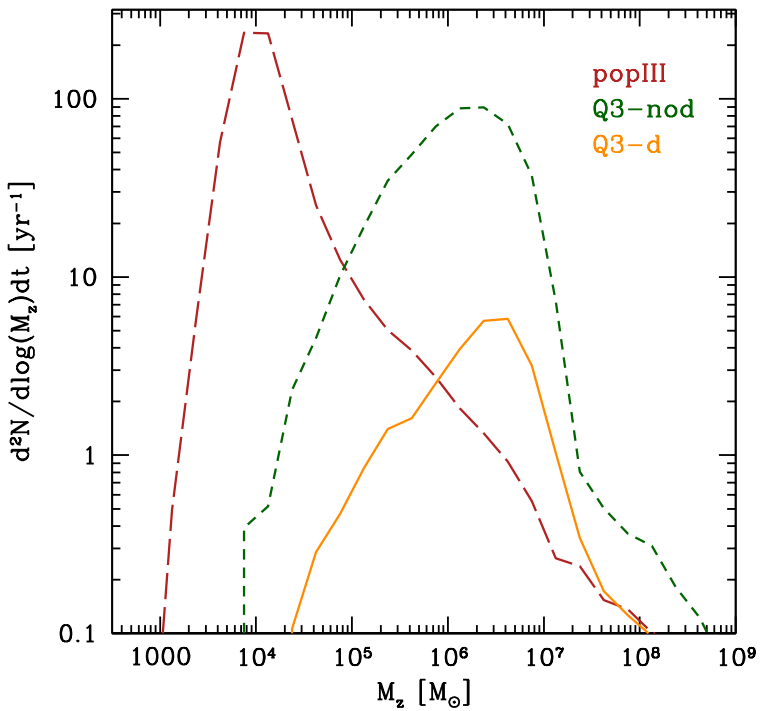

[AK+ (arXiv: 1511.05581)]

Parameter Estimation

We used Fisher matrix analysis to compute measurement errors on the binary parameters, using spin-precessing inspiral-only circular waveforms with higher harmonics.

We computed the SNR ratio between IMR phenomC and inspiral-only waveforms.

We rescaled the measurement errors on extrinsic parameters using results from data analysis performed on a few spin-precessing IMR hybrid waveforms.

Most intrinsic parameter measurements are not significantly affected by the merger and ringdown, whereas the sky location and distance measurement are.

Measurement Error Gain

The distance measurement will scale like the SNR ratio, and the sky location will scale like the square of the SNR ratio.

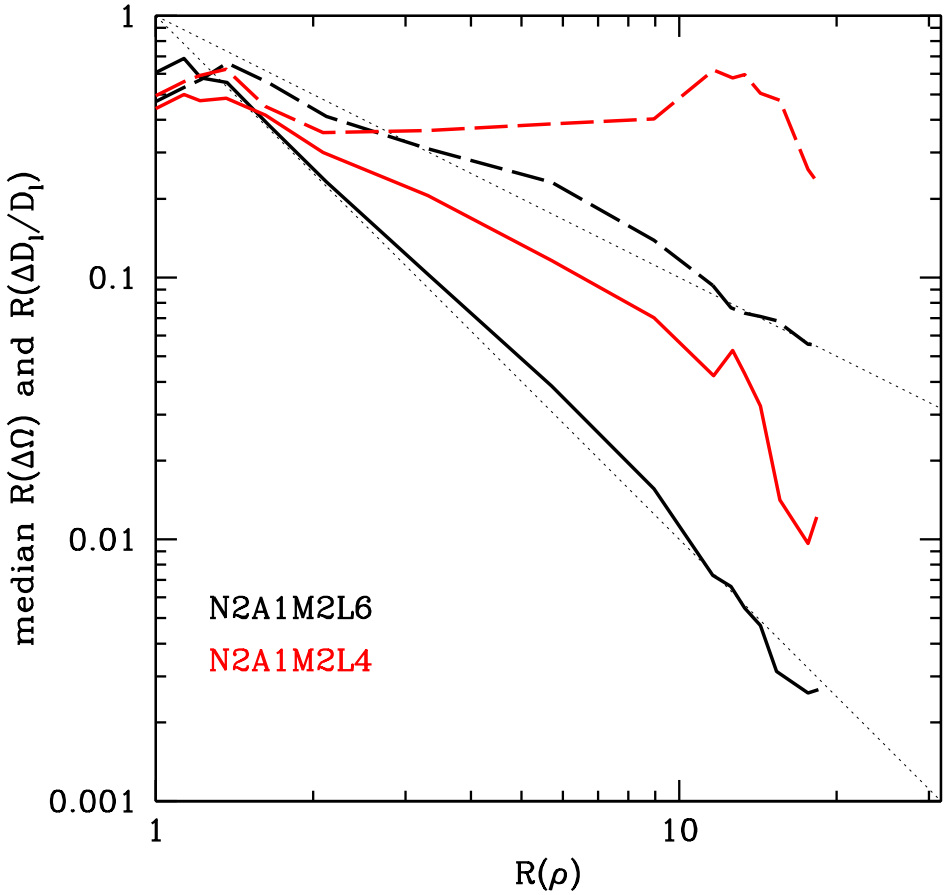

[AK+ (arXiv: 1511.05581)]

Detections from astrophysical populations

The number of detections for a five-year mission varies from model to model. We expect several tens to several hundred.

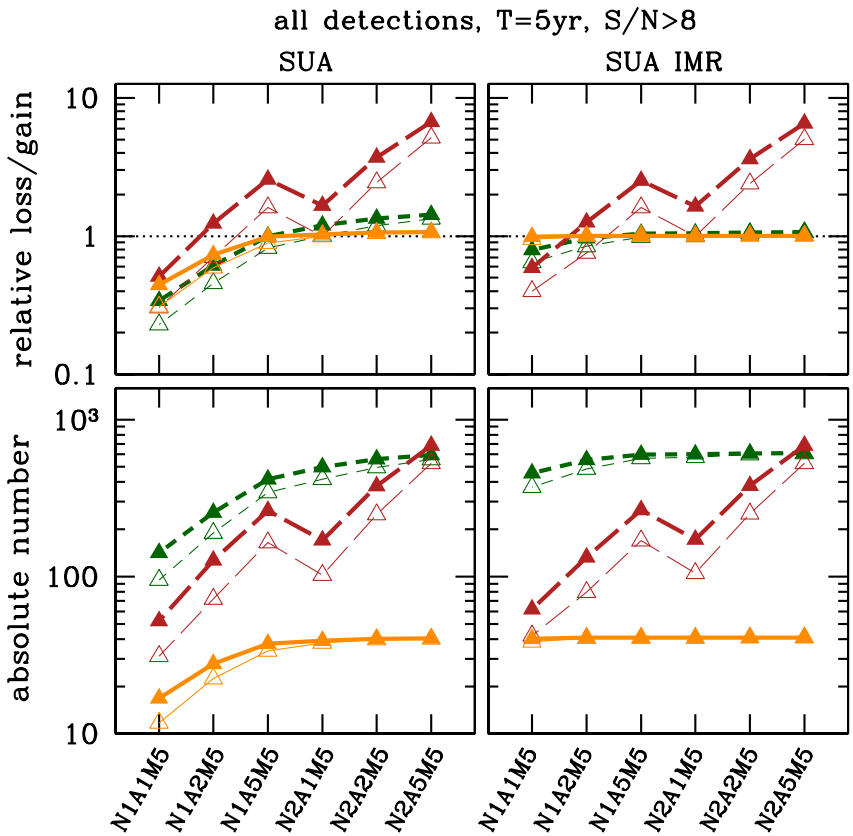

[AK+ (arXiv: 1511.05581)]

Mass measurement

For about a third of systems, we will be able to measure the individual masses with a precision better than 10^{-2}.

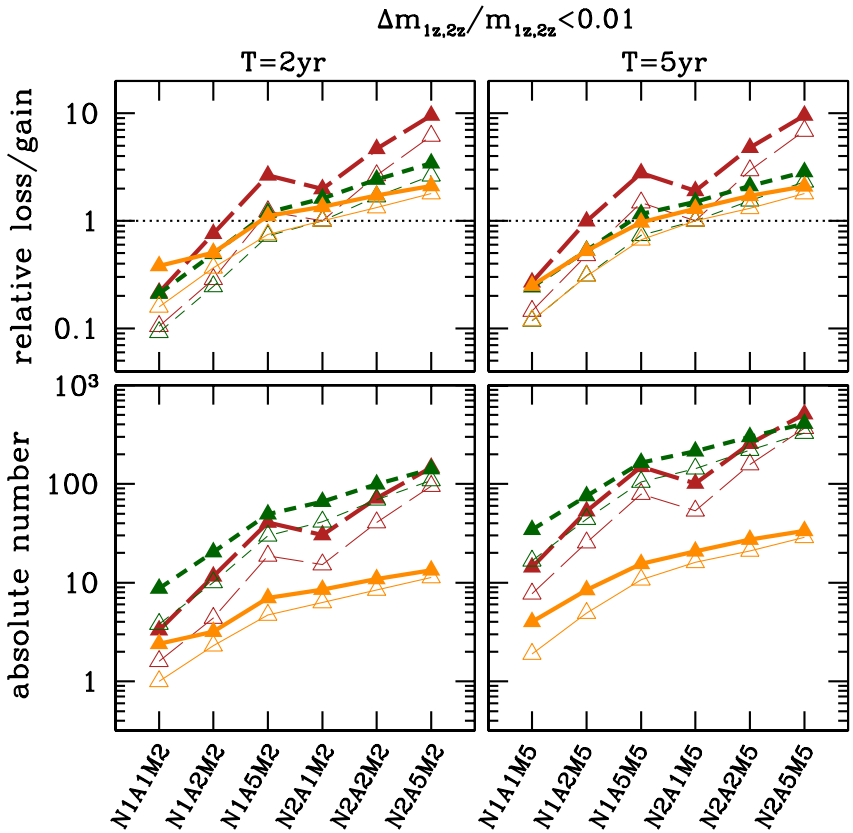

[AK+ (arXiv: 1511.05581)]

Spin measurement

In favourable conditions, the spin of the primary will be able to be measured at the level of 10^{-2}, and the spin of the secondary at the level of 10^{-1}.

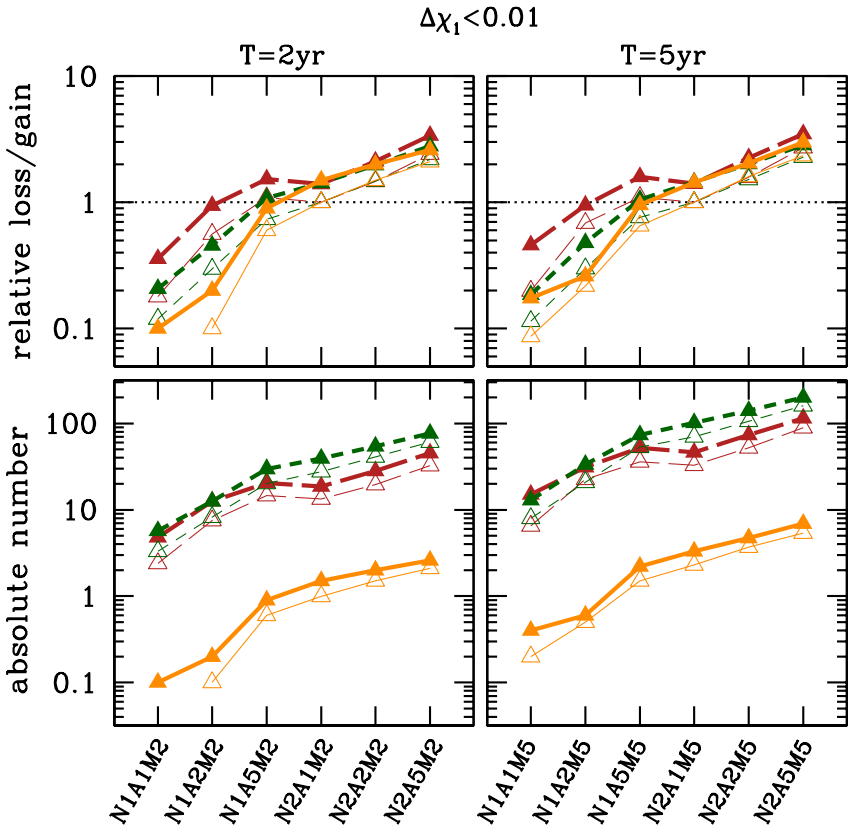

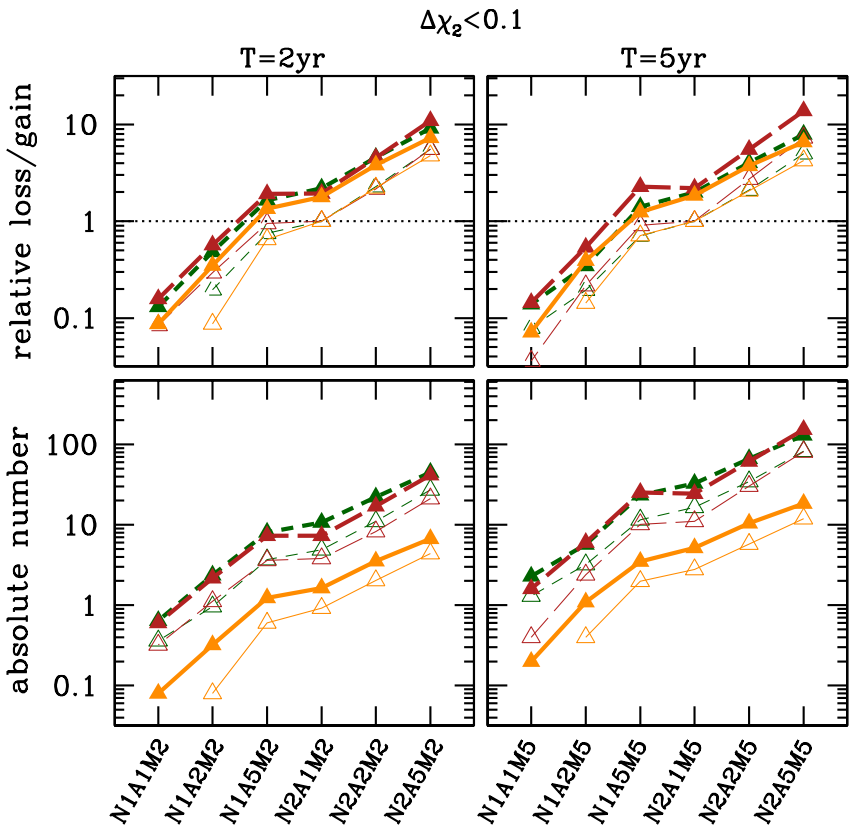

[AK+ (arXiv: 1511.05581)]

Spin alignment angle

The spin alignment angle will be measurable to within 10 degrees for a significant fraction of the observations.

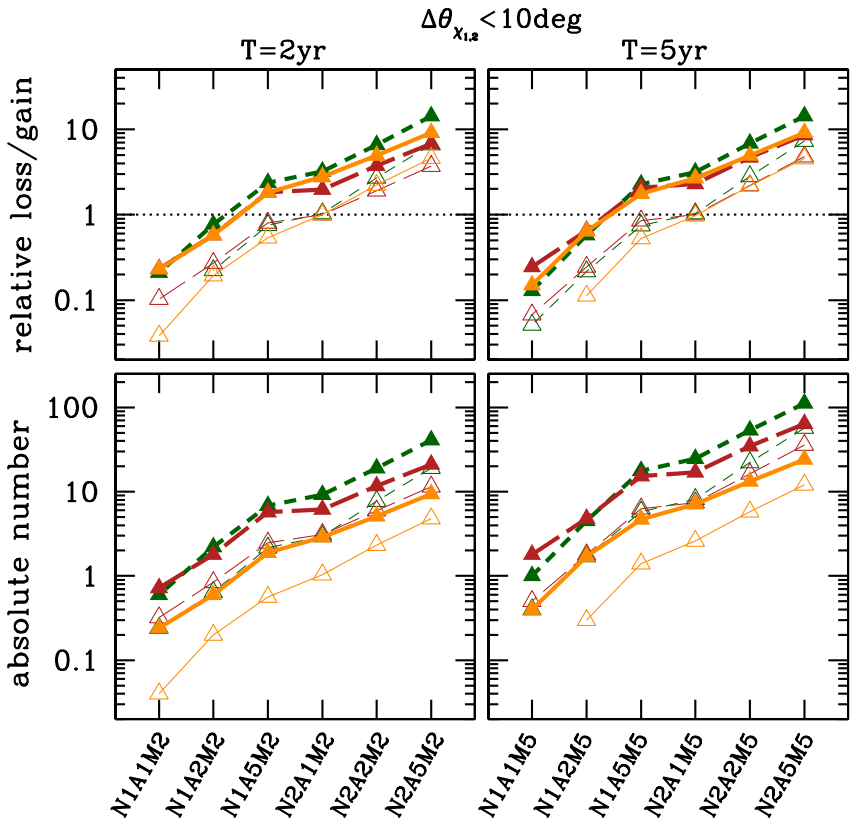

[AK+ (arXiv: 1511.05581)]

Cosmology

A significant fraction of the systems will allow for a sky localization good enough to identify the host galaxy with contemporary detectors, with 10% distance measurement accuracy at low redshift, in order to constrain cosmological parameters.

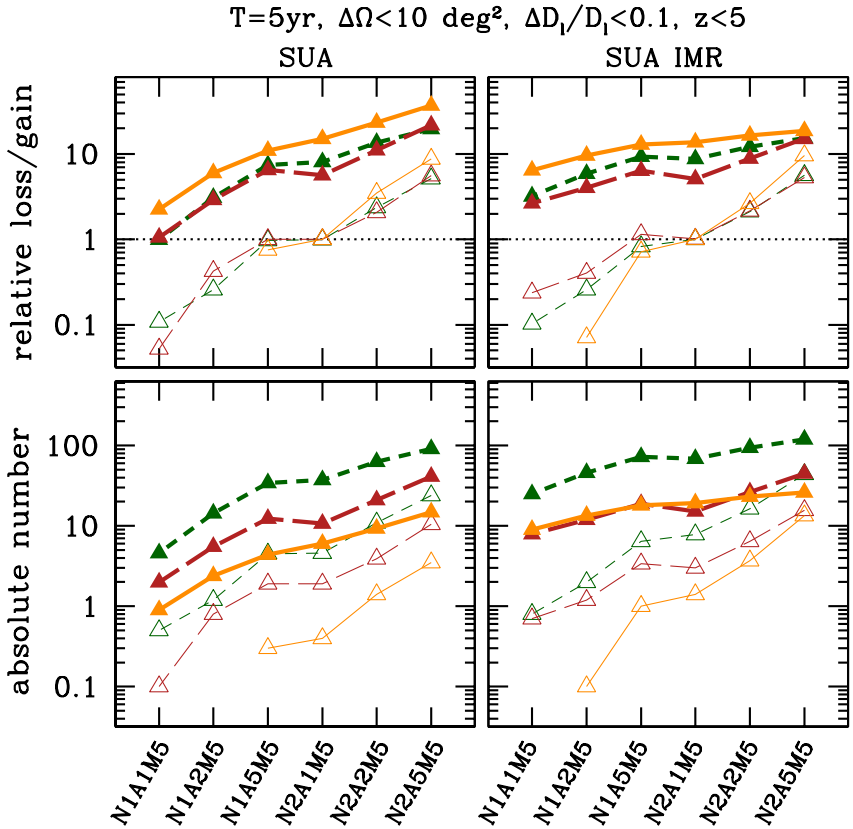

[AK+ (arXiv: 1511.05581)]

Early Universe

Depending on the model, a few to a few hundred systems will be correctly identified at high redshift, allowing to probe SMBH evolution models.

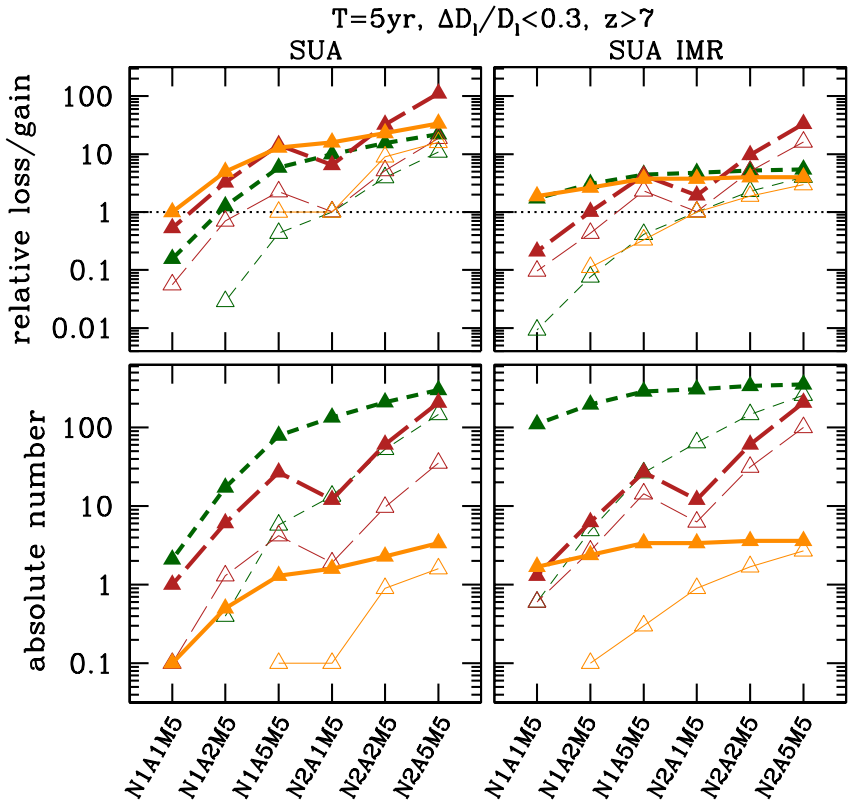

[AK+ (arXiv: 1511.05581)]

Eccentricity

The physics driving the final merger of a SMBHB resulting from a galaxy merger will influence the characteristics of the binary signal.

In particular, if gas dynamics cannot drive the merger by themselves, triple interactions will then drive the final merger, which will tend to increase the orbital eccentricity of the system.

In particular, if not enough stars are present in the binary's neighbourhood, the binary can stall. When another another galaxy merger occurs, a third SMBH will form a hierachical triplet with the inner binary.

Eccentricity

Kozai-Lidov oscillations can drive the merger by increasing the orbital eccentricity.

Triple interactions can also increase the eccentricity of the binary by ejecting the lighter component of the triple.

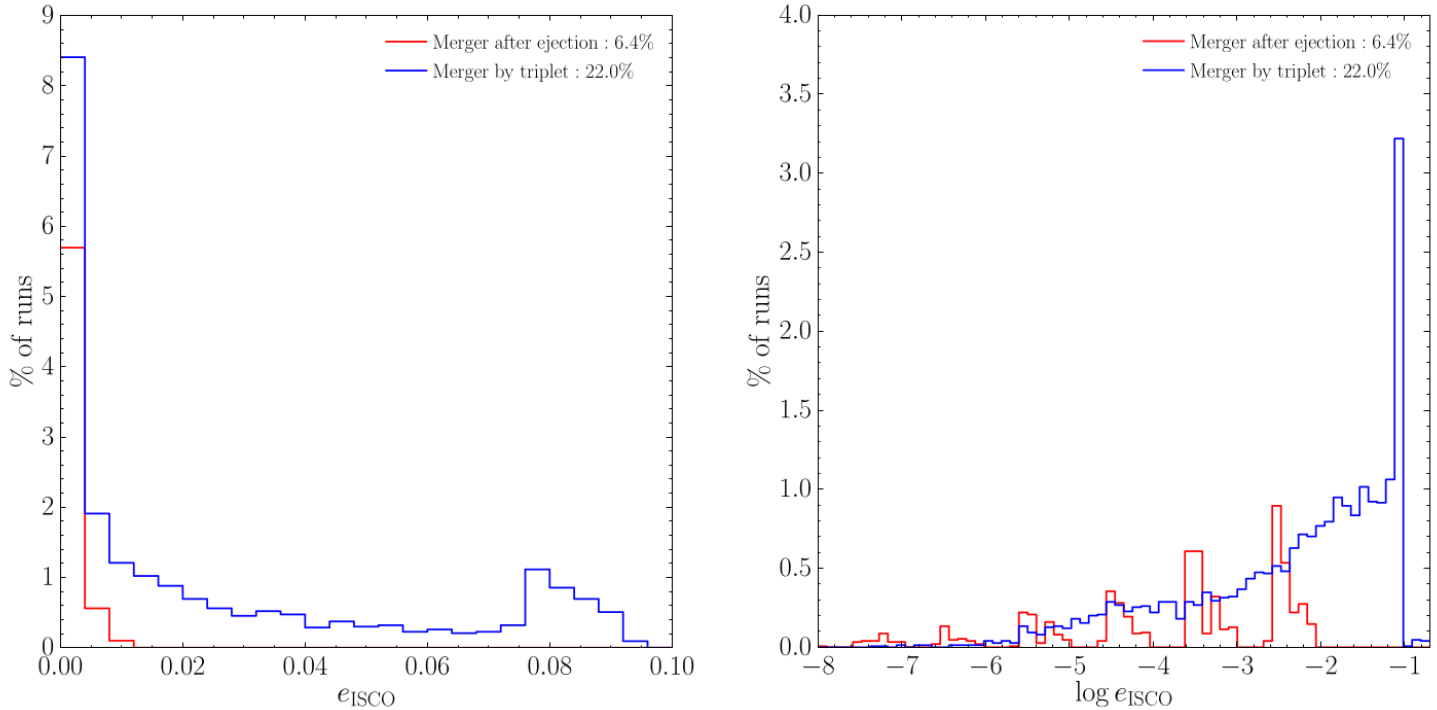

[Bonetti+ (arXiv:1709.06088)]

Eccentricity

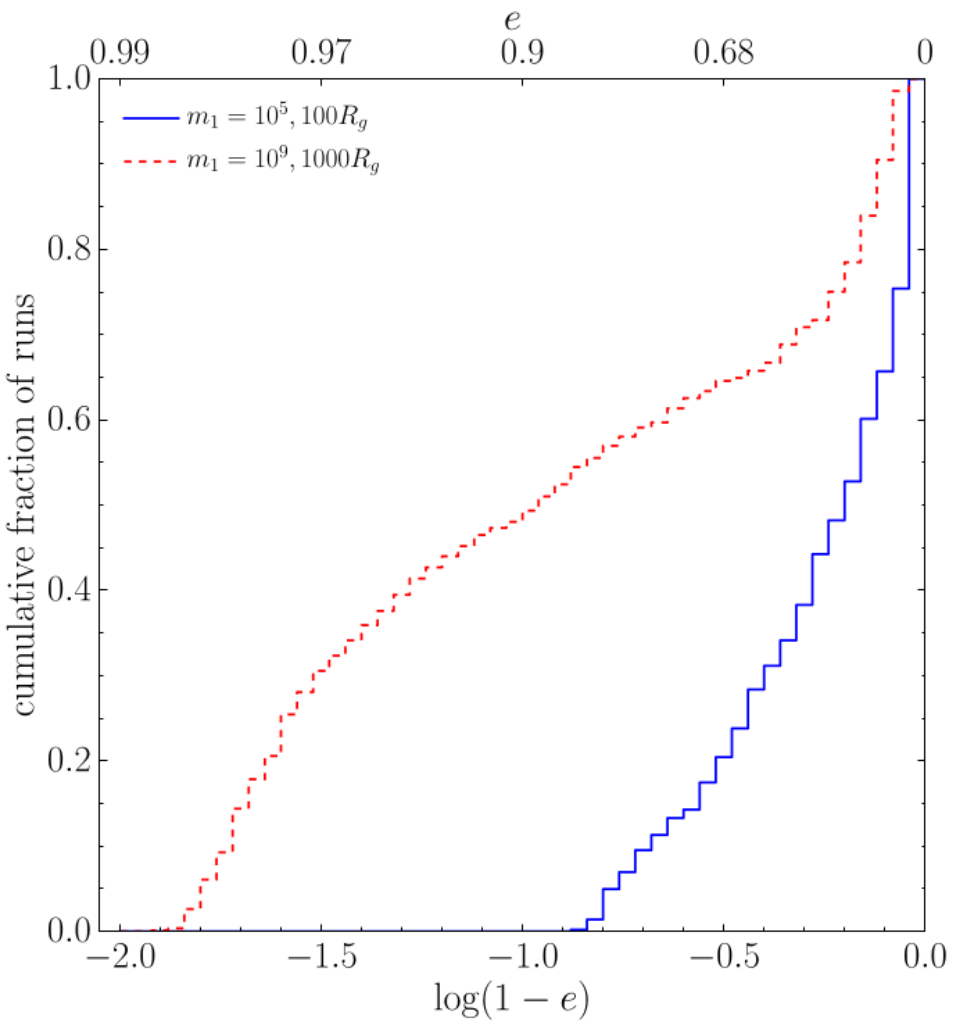

[Bonetti+ (arXiv:1709.06088)]

Ringdown measurement

High SNRs will allow the simultaneous detection of multiple ringdown modes, allowing Kerrness tests for the remnant objects.

The bucket of the LISA noise curve corresponds to the ringdown frequencies of Sagittarius A*-type black holes.

Ringdown measurement

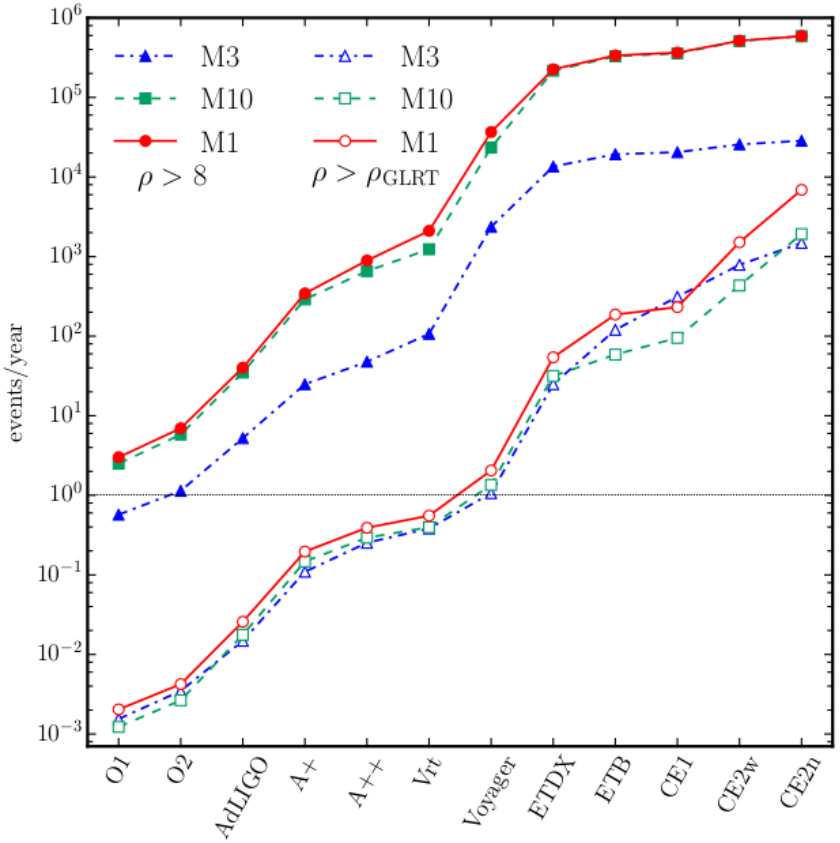

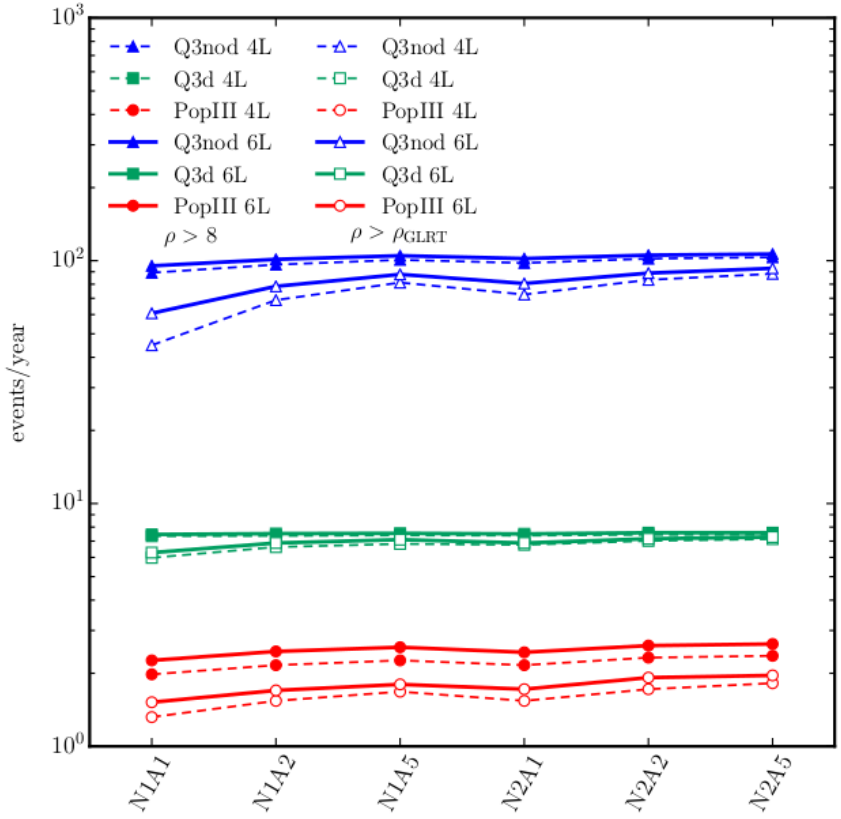

[Berti+ (arXiv:1605.09286)]

Axion-like particles

The presence of ultralight bosons such as QCD axions ($m_b \sim 10^{-17}$ eV - 10^{-13} eV) will trigger superradiant instabilities in SMBHs.

This happens when particle pairs are created in the ergoregion, one of which carries negative energy and falls into the black hole. Depending on the mass of the boson, the mass of the SMBH, and its spin, this process will enter a resonance and drain significant angular momentum from the SMBH.

By measuring the spins and masses of binary components, we can detect holes in the mass-spin plane that would be a signature of the presence of such bosons.

LISA will allow us to either reject ultralight bosons in a certain mass range, or if present to detect them and measure their mass with $\sim 10\%$ accuracy.

Black hole populations

Simulation of a heavy mass seed model in the presence of an ultalight boson of mass $m_b = 10^{-16} eV$. The shape of the hole in the mass-spin plane is characteristic of this boson mass.

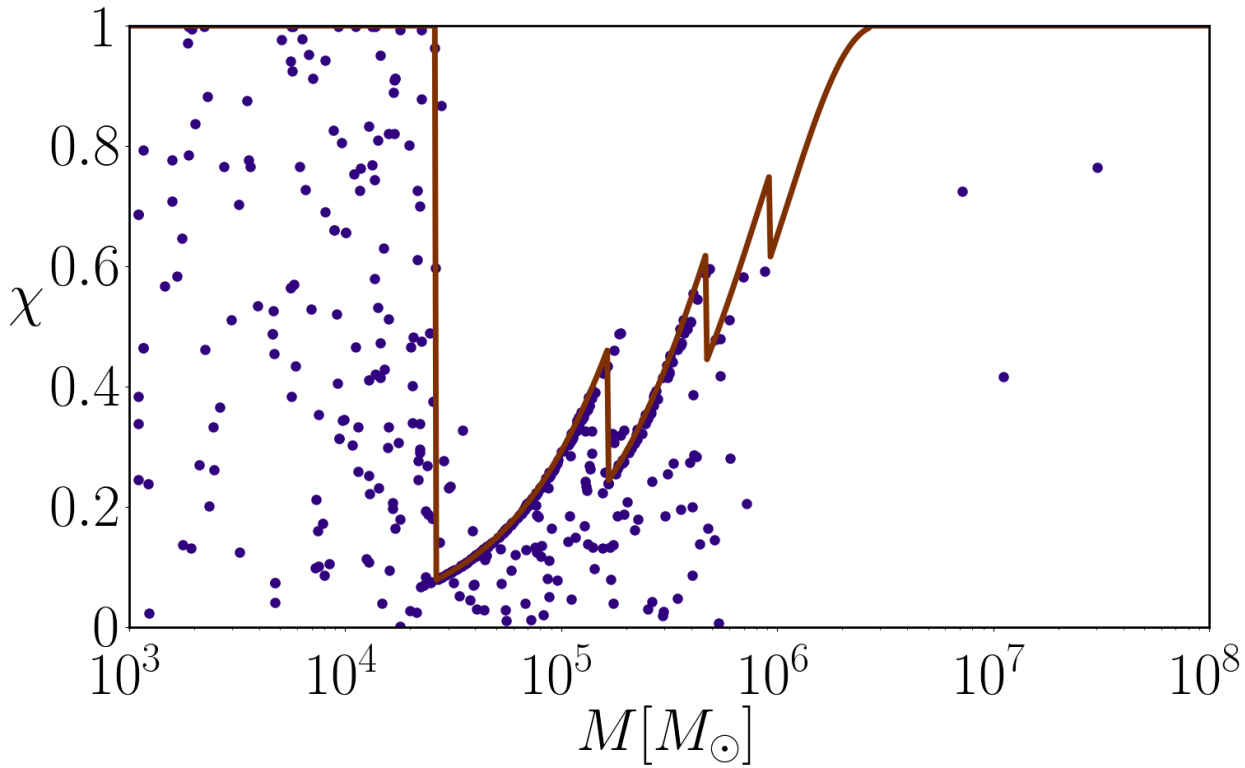

[Brito+ (arXiv:1706.06311, 1706.05097)]

Boson mass rejections

Supposing that such particles do not exist, LISA can reject boson masses in a certain mass range after a few observations.

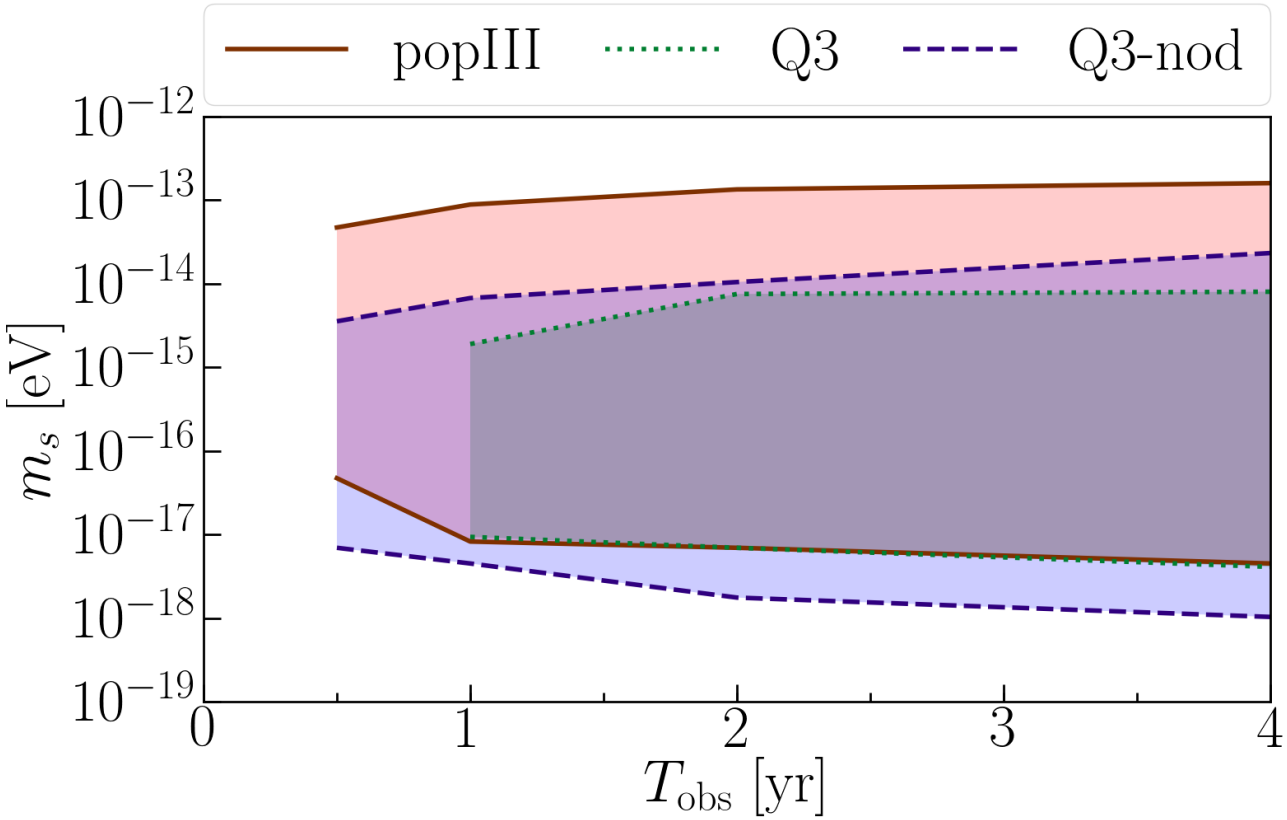

[Brito+ (arXiv:1706.06311, 1706.05097)]

Challenges in waveform modelling: Galactic binaries

- Due to the quasimonochromatic nature of these sources, these are fairly simple to model, even when taking into account the full LISA response.
- The effect of the eccentricity on the gravitational waveform has yet to be studied.
- Additional effects can be important: Kozai-Lidov resonances, mass transfer, etc.

Challenges in waveform modelling: EMRIs

- In order to reduce the orbital phasing error along the whole inspiral to less than a cycle, self-force calculation at second order in the mass ratio are needed.
- The rich structure of the waveform requires the development of new, efficient algorithms to compute the gravitational waveforms.

Challenges in waveform modelling: IMRIs

- BHB waveforms are efficient for modelling systems with mass ratios of 1 to 1/50.
- EMRI waveforms are efficient for modelling systems with mass ratios higher than 10^{-4}.
- In the intermediate mass ratio regime 10^{-2} - 10^{-4}, we don't have efficient waveforms to perform our analyses.

Challenges in waveform modelling: Stellar-mass BHBs

- In order to probe binary formation models, the development of eccentric waveforms is important.
- Since these systems are in the early inspiral, post-Newtonian waveforms are appropriate.
- Since these systems are located at the higher end of the frequency band, the inclusion of the full LISA response is crucial.
- The structure of the signal requires the development of very fast eccentric waveforms.

Challenges in waveform modelling: SMBHBs

- Because we expect high signal-to-noise ratios, highly accurate waveforms are required.
- In particular, the inclusion of multiple ringdown modes, eccentricity, and spin-precession are all important.
- For binary masses $M \lesssim 10^5 M_\odot$, the inclusion of the full LISA response will be important, in particular the merger and ringdown response.
- Very high eccentricities are predicted by some scenarios, which require a novel way of modelling binary waveforms.